Scribble mutation disrupts convergent extension and apical constriction during mammalian neural tube closure.

Alyssa C. Lesko[1*], Raymond Keller[2], Ping Chen[3], and Ann Sutherland[1]

[1]Department of Cell Biology, University of Virginia Health System, Charlottesville, VA, 22908, USA

[2]Department of Biology, University of Virginia, Charlottesville, VA, 22903, USA.

[3]Otogenetics Corporation, Atlanta, GA 30360.

*Corresponding author: Alyssa C. Lesko (al8th@virginia.edu)

Abstract

Morphogenesis of the neural tube in vertebrates relies on elongation and bending of the neural plate epithelium, which is driven at the cellular level by polarized cell intercalation, cell shape changes, and the underlying cytoskeletal dynamics that promotes these behaviors. Mutations of the gene encoding *Scribble* (*Scrib*) lead to neural tube defects in mice, however the cellular and molecular mechanisms by which *Scribble* regulates neural cell behavior remain unknown. Our analysis of neural development in *Scribble* mutants characterizes several defects in overall tissue shape changes. Live cell imaging of mouse embryos revealed that the *Scrib* mutation leads to defects in polarized cell intercalation and rosette resolution, as well as loss of apical constriction and cell wedging. *Scrib* mutant embryos displayed aberrant localization and expression of the junctional proteins ZO-1, Par3, Par6, aPKC, and cadherins, as well as the cytoskeletal proteins actin and myosin. These findings identify a novel role for Scrib in regulating neural cell behavior during NTC and further our understanding of the molecular mechanisms involved in mammalian neural development.

Key Words: Convergent Extension, Apical Constriction, Neural Tube Closure, Scribble, Planar Cell Polarity

Introduction

Neural tube development in vertebrates begins with the elongation of the neural plate, followed by the bending, folding, and fusion of the tissue into a tube (Sadler, 2005, Nikolopoulou et al., 2017). In mice, a zippering mechanism of neural tube closure (NTC) is initiated sequentially at three sites, closure 1 at the hindbrain/cervical boundary, closure 2 at the forebrain/midbrain boundary, and closure 3 at the most rostral point of the forebrain (Sadler, 2005, Nikolopoulou et al., 2017). From these 3 sites closure occurs by zippering in both directions to close the length of the neural tube (Copp and Greene, 2010, Sadler, 2005, Nikolopoulou et al., 2017). Failure of these closure and zippering mechanisms can result in severe birth defects depending on where the failure occurs

(Greene and Copp, 2014, Copp and Greene, 2013). For example, failure of closure in the spinal region results in spina bifida, whereas failure of zippering between closure 2 and 3 result in exencephaly or anencephaly (Copp and Greene, 2013). Failure of closure along the entire axis resulting in open brain and spinal cord is classified as craniorachischisis (CRN) (Copp and Greene, 2013). All of these neural tube defects (NTD) affect quality of life, and can result in death at or before birth.

Elongation of the neural plate during NTC is driven by convergent extension (CE), and the bending and closure of the neural epithelium is promoted by apical constriction and cell shape changes (reviewed in (Sutherland et al., 2020, Nikolopoulou et al., 2017)). During CE cells intercalate mediolaterally (ML) to extend the tissue in the anterior-posterior (AP) direction (Keller, 2002). This process was first demonstrated in *Xenopus* mesodermal tissue and in the ascidian notochord, where cells use mediolaterally oriented protrusions to crawl between neighboring cells to intercalate, elongating the tissue in the anterio-posterior dimension (Keller, 2002, Munro and Odell, 2002). Studies in *C. elegans* showed that epithelial cells could use a similar mechanism (Williams-Masson et al., 1998), while analysis of germ band extension in Drosophila uncovered novel mechanisms for epithelial tissue elongation involving rearrangement of apical intercellular junctions through a T1 process or through rosette formation (Bertet et al., 2004, Blankenship et al., 2006). In the mouse, neural epithelial cells were found to intercalate using a combination of polarized basal mediolateral protrusive activity and apical junctional rearrangements (Williams et al., 2014), and later work in Drosophila confirmed that germ band elongation is also driven by a combination of basolateral protrusive activity and apical junctional rearrangement (Sun and Amourda, 2017). As the tissue elongates anterio-posteriorly, cells in the neural plate constrict their apical surface while elongating and orienting their basal ends mediolaterally to form wedge shaped cells (Suzuki et al., 2012, Moury and Schoenwolf, 1995). These cell shape changes are thought to provide the mechanical force necessary for the bending and zippering of the neural plate (Inoue et al., 2016, Nikolopoulou et al., 2017).

The planar cell polarity (PCP) pathway, which regulates the planar orientation of cells within a tissue, has been shown to affect NTC through orientation of cell intercalation and promotion of apical constriction (Heisenberg et al., 2000, Tada and Smith, 2000,

Wallingford et al., 2000, Wallingford and Harland, 2001, Axelrod and McNeill, 2002, Williams et al., 2014, López-Escobar et al., 2018, Ybot-Gonzalez et al., 2007). Mutation of genes encoding PCP components such as Frizzled (Fz3/Fz6 or Fz2/7), Van Gogh-like (Vangl1/Vangl2), and Dishevelled (Dvl1/2/3) in mice cause open neural tube and CRN (Kibar et al., 2001, Murdoch et al., 2001a, Wang et al., 2006b, Hamblet et al., 2002, Wang et al., 2006a). For example, *Vangl2 Looptail* (*Vangl2*^{Lp}) mice, which contain a point mutation in the *Vangl2* gene that prevents delivery of Vangl2 to the plasma membrane (Kibar et al., 2001, Murdoch et al., 2001a, Merte et al., 2010), and truncation mutants of the Protein tyrosine kinase 7 (*Ptk7)* gene exhibit disrupted CE and NTC (Williams et al., 2014). The PCP pathway regulates morphogenesis and NTC by regulating cytoskeletal dynamics through Rho kinase signaling (reviewed in (Coravos et al., 2017, Heer and Martin, 2017, Sutherland and Lesko, 2020)). In chick embryos, actin, myosin II, and Rho accumulate at apical ends of cells prior to neural plate bending, and inhibition of actin polymerization and myosin activity result in failure of NTC (Kinoshita et al., 2008). Similarly, in the mouse neural plate inhibition of Rho kinase and of actin disassembly inhibits NTC through effects on cell shape and apical constriction (Ybot-Gonzalez et al., 2007, Williams et al., 2014, Butler et al., 2019), and Rho kinase inhibition in *Vangl2*$^{Lp+/-}$ embryos exacerbates NTD (Escuin et al., 2015, Ybot-Gonzalez et al., 2007). Furthermore, mutation of *Ptk7* disrupts myosin IIB organization in mouse neural cells (Williams et al., 2014), and affects signaling to Rho kinase (Andreeva et al., 2014). The PCP pathway thus regulates cytoskeletal dynamics and Rho signaling to promote NTC through junctional rearrangement, cell shape changes, and biomechanical accommodation of neural fold zippering (Galea et al., 2017, Galea et al., 2018).

Scribble (Scrib) acts as a scaffold for formation of protein complexes at the plasma membrane which are involved, particularly in epithelia, in apical-basal and planar polarization of the cell (Bonello and Peifer, 2018). Scrib contains an amino-terminal LRR region important for its correct localization to the plasma membrane and for its role in regulating apical-basal polarity and junctional composition (Kallay et al., 2006, Bonello and Peifer, 2018). At the carboxy terminus, Scrib has four PDZ binding domains important for protein-protein interactions including domains that directly interact with Vangl2 and the PCP pathway (Kallay et al., 2006). Mutations in *Scrib* result in CRN in both mice and

humans (Murdoch et al., 2003, Robinson et al., 2012, Lei et al., 2013, Zarbalis et al., 2004, Kharfallah et al., 2017). Scrib's role in neural tube development has been predominantly studied in two mouse models: *Scribble Circletail* (*Scrib*^{Crc}) (Murdoch et al., 2003) and *Scribble Rumplestiltzchen (Scrib*^{rumz}*,* also published as Line 90, *Scrib*^{L90}*)* (Zarbalis et al., 2004, Dow et al., 2007)*,* both of which display CRN and short body axis phenotypes. The *Scrib*^{Crc} mutation is a frameshift mutation in the PDZ domain causing truncation of Scrib and loss of expression (Murdoch et al., 2003). The *Scrib*^{rumz} mutant contains a point mutation in the N-terminal LRR domain that leads to mislocalization and decreased protein stability (Zarbalis et al., 2004). Both *Scrib*^{Crc} and *Scrib*^{rumz} mutants genetically interact with the *Vangl*^{Lp} mutant to cause CRN (Murdoch et al., 2001b, Zarbalis et al., 2004), though the underlying mechanisms are not fully understood.

Here we show that mutation of *Scrib* leads to specific defects in CE and apical constriction during NTC and affects the molecular composition of the apical junctions. In particular, we find that *Scrib*^{rumz} affects cell intercalation behavior similarly to *Ptk7*^{XST87}, but differently from *Vangl2*^{Lp}, suggesting that the genetic interaction between *Scrib* and *Vangl2*^{Lp} results from complementary effects of these two mutations on cell behavior. Interestingly, we also find that the genetic interaction between *Scrib*^{rumz} and *Vangl2*^{Lp} is qualitatively different from that between *Scrib*^{rumz} and a *Vangl2* knockout allele. These results clarify the cellular and molecular mechanisms by which Scrib regulates NTC.

Materials and Methods

Animals

Scrib^{rumz} (also known as *Scrib*^{L90}) mice (Zarbalis et al., 2004), and *Scrib*^{Crc} mice (Murdoch et al., 2003), were obtained from Dr. Xiaowei Lu, University of Virginia, and kept as heterozygous stocks in our colony. The *Scrib*^{rumz} mutant contains a point mutation in the N-terminal LRR domain (Zarbalis et al., 2004) that affects both the stability of the protein and its ability to localize to the membrane (Dow et al., 2007), while the *Scrib*^{Crc} mutation is a loss of function frameshift mutation in the Scrib C-terminus PDZ binding domains causing loss of expression of Scrib (Murdoch et al., 2003). *Vangl2*^{Lp} mice, exhibiting a

point mutation that causes Vangl2 to be sequestered in the endoplasmic reticulum and not properly targeted to the membrane, were obtained from The Jackson Lab and kept as heterozygous stocks in our colony (Kibar et al., 2001, Merte et al., 2010). *Vangl1*$^{co/co}$ and *Vangl2*$^{co/co}$ conditional knockout mice were obtained from Dr. Jeremy Nathans, Johns Hopkins University and Dr. Yingzi Yang, NIH, respectively (Chang et al., 2016, Song et al., 2010), and kept as homozygotes in our colony. *Tg(Sox2-cre)1Amc/J (Sox2Cre*) females, obtained from The Jackson Lab, were crossed to *Vangl1*$^{co/co}$ and *Vangl2*$^{co/co}$ conditional males to produce *Vangl1*$^{KO/+}$ and *Vangl2*$^{KO/+}$ heterozygotes. *Vangl2*$^{GFP/GFP}$ mice, containing GFP labelled Vangl2, were obtained from Dr. Ping Chen, Emory University School of Medicine (Qian et al., 2007), and crossed to *Scrib*$^{rumz/+}$ mice to produce *Scrib*$^{rumz/+}$*; Vangl2*$^{GFP/+}$heterozygotes. B6.129(Cg)-*Gt(ROSA)26Sortm4(ACTB-tdTomato,-EGFP)Luo*/J (*mT/mG*) mice carrying floxed membrane-targeted Tomato fluorescent protein followed by membrane-targeted eGFP (Muzumdar et al., 2007) were obtained from The Jackson Lab and maintained as homozygotes in our colony. All animals were genotyped with PCR using the primers listed in Supplementary Table 1 and the genotype of *Scrib*^{Crc} and *Scrib*^{rumz} embryos were confirmed by sequencing. Crosses were set-up between males and females of desired strains and the morning a plug was identified was designated as E0.5. Embryos were dissected at the desired stage in Whole Embryo Culture Medium (WECM) (Yen et al., 2009). All animal use protocols were in compliance with PHS and USDA guidelines for laboratory animal welfare and reviewed and approved by the University of Virginia Institutional Animal Care and Use Committee.

Live imaging

To view CE and cell behavior, male *Scrib*$^{rumz/+}$*; mT/mG* mice, were mated to female *Scrib*$^{rumz/+}$*; Sox2Cre* mice in order to induce recombination and expression of membrane eGFP in all cells of all embryos, due to the maternal effect of the Sox2Cre (ref). Live imaging was carried out as previously described (Williams et al., 2014). Briefly, embryos were dissected at the 1-3 somite stage and cultured in a mixture of 50% WECM and 50% rat serum. Embryos were mounted distal tip down in a glass-bottomed chamber, covered with culture medium which was then overlaid with mineral oil to prevent evaporation, and

placed on the Zeiss 510 or Leica SP8 confocal microscope in the University of Virginia Keck Center (PI:AP; NIH-RR025616) in an environmental chamber at 37˚C and 5% CO_2 gas. For CE and cell behavior analysis, embryos were imaged for 6-10 hours at an interval of 6min at 40x with Z-stacks of 10-15 planes captured at 2μm intervals. All embryos were lysed and genotyped either by PCR or by sequencing after imaging.

Image Analysis

In order to best visualize the Z-plane of interest in the tissue for CE analysis confocal stacks were aligned by concatenating single optical sections across time. Movies were also aligned in the X and Y axes using the Stackreg plugin in Image J to eliminate whole embryo drift from cell tracking results. Rectangular distortion diagram boxes, oriented with their long axis parallel to the AP axis of the neural plate, were generated from cell tracking of neural plate cells throughout live imaging movies. Image J was then used to calculate the CE index, which is represented by the change in the aspect ratio of the length of the AP axis (length of boxes) over the width of the ML axis (width of the boxes). The change in AP length represents the amount of elongation, while the change in ML width represents the amount of convergence. For intercalation analysis cells were manually tracked and observed in clusters of approximately 10 cells in order to evaluate intercalation frequency and the polarity of separation of neighboring cells. Individual cells were measured to analyze basal and apical area and apical constriction index (ACI), ratio of basal cell area over apical cell area, as well as basal orientation by fitting an ellipse to each cell at both the basal and apical surfaces

Immunofluorescence staining

For immunofluorescence whole mount staining of E8.5 embryos were fixed in 3.7% paraformaldehyde for 2 hours. Following fixation, embryos were washed overnight in 1xtsPBS (0.5% triton + 0.1% saponin in 1 x PBS), blocked for 1 hour at 37ºC in 10% goat serum in 1x tsPBS, and incubated in the following primary antibodies diluted 1:100 (except phalloidin, 1:300) in blocking solution overnight at 4ºC: aPKC (sc-216, SCBT) ,

ZO-1 (21773-1-AP, proteintech), E-cad (610181, BD), N-cad (610920, BD), Par3 (07-330, Millipore), Par6 (sc-166405, Santa Cruz), rhodamine phalloidin (R415,Invitrogen), Myosin IIA (PRB-440P,Covance), and Myosin IIB (PRB-445P,Covance). Following primary incubation, embryos were washed in 1xtsPBS and incubated in the following Alexa-conjugated secondary antibodies 1:200 in blocking solution overnight at 4ºC: Alexa-Fluor donkey anti-rabbit IgG 488 (A21206, Life Tech), Alexa-Fluor goat anti-mouse IgG 546 (A11030, Life Tech), Alexa-Fluor goat anti-rabbit IgG 647 (A21245, Life Tech), and Alexa-Fluor donkey anti-mouse IgG 488 (A21202, Life Tech). Embryos were washed with 1x tsPBS and imaged on Zeiss 780 confocal microscope in the University of Virginia Keck Center (PI: AP; NIH-ODO16446). Zen software was used to acquire images and Image J was used to analyze images.

Western Blot

For analysis of whole cell lysates, whole embryos were lysed directly in Laemmli sample buffer, subjected to SDS-PAGE, transferred to nitrocellulose membrane, blocked in 1% FG in 1xTBST 1 hour at 4ºC, and analyzed by Western blotting with Scrib primary antibody (A01651, Boster Bio) 1:1000 in blocking solution incubated overnight at 4ºC. Protein was visualized with the following IRDye conjugated secondary antibodies 1:20,000 in 1xTBST + 0.01% SDS for 45min at room temperature: rabbit680rd and mouse800cw (LiCor). Tubulin was used as the loading control. LiCor Image Studio software was used to acquire and analyze images.

Statistics

PAST software (https://folk.uio.no/ohammer/past/) was used to make rose diagrams and to perform the associated circular statistics including circular mean and Rao's spacing test. Graphpad Prism 8 software was used to create all bar graphs and was used to perform all other statistical analyses including Chi-square, one-way ANOVA and two-way ANOVA tests.

Results

Scrib^{rumz} and Scrib^{Crc} mutants exhibit similar phenotypes of open neural tube and lack of axial turning.

The *Scrib^{rumz}* mutant has not been characterized in detail, so to compare effects of this mutation, which reduces Scrib expression and localization ((Dow et al., 2007) and Supplemental Figure 1), and the *Scrib^{Crc}* truncation mutation, which is an effective null ((Murdoch et al., 2014) and Supplemental Figure 1), E11.5 embryos were dissected and imaged to examine phenotypes (Figure 1A). The overall incidence of NTD was similar between the two mutants: 81% of *Scrib$^{rumz/rumz}$* and 88% of *Scrib$^{Crc/Crc}$* mutant embryos display neural tube defects (NTD) while only 4% of *Scrib$^{rumz/+}$* and 2% of *Scrib$^{Crc/+}$* heterozygous embryos exhibit NTD (Figure 1A,B). However, a finer-grained analysis of the phenotypes revealed differences between the two mutant strains. Phenotypes were further classified as normal, kinked tail, developmental delay (E9-10), brain closure defect (anencephely), abdominal wall defect (omphalocele), open neural tube (ONT) (CRN), or ONT with axial torsion (a twist in the body axis due to incomplete turning) (Figure 1C). The distribution of abnormal phenotypes is significantly different between *Scrib$^{rum/rumz}$* and *Scrib$^{Crc/Crc}$* mutants where *Scrib$^{Crc/Crc}$* mutant phenotypes are more severe with a larger percentage of embryos displaying ONT (Figure 1C). However, a larger percentage of *Scrib$^{rumz/rumz}$* mutant embryos display axial torsion at 69% compared to 57% of *Scrib$^{Crc/Crc}$* embryos (Figure 1C). Minor defects were observed in 20-40% of wildtype and heterozygous. *Scrib$^{Crc/Crc}$* and *Scrib$^{rumz/rumz}$* embryos do not have complete penetrance of ONT, as was previously described for *Scrib$^{Crc/Crc}$* (Figure 1C and (Murdoch et al., 2001b, Zarbalis et al., 2004, Murdoch et al., 2014)), likely due to the mixed backgrounds of the transgenic lines in our colony which has been previously demonstrated to influence the severity of NTD in *Scrib$^{Crc/Crc}$* mutants (Murdoch et al., 2014).

Scrib mutants exhibit different genetic interactions with Vangl2^{Lp} and *Vangl2^{KO}*.

Both *Scrib*^{rumz} and *Scrib*^{Crc} mutations interact genetically with the *Vangl2*^{Lp} mutation to cause ONT (Murdoch et al., 2001b, Zarbalis et al., 2004). To more completely characterize the phenotypes resulting from *Scrib* and *Vangl2* genetic interactions, phenotypes of *Scrib*^{rumz}*; Vangl2*^{Lp} and *Scrib*^{Crc}*; Vangl2*^{Lp} embryos were compared and the genetic interactions between *Scrib* mutants and Vangl1 knockout (*Vangl1*^{KO}) and Vangl2 knockout (*Vangl2*^{KO}) were examined at stage E11.5 (Figure 2A). Consistent with previous studies *Scrib*$^{rumz/+}$*; Vangl2*$^{Lp/+}$ and *Scrib*$^{Crc/+}$*; Vangl2*$^{Lp/+}$ double heterozygous embryos display a small but significant increase in the percentage of embryos with NTD, 16% and 13% respectively, compared to wildtype (Figure 2B, (Murdoch et al., 2001b)). Interestingly, loss of one allele of either Vangl1 (*Vangl1*$^{KO/+}$) or Vangl2 (*Vangl2*$^{KO/+}$) has no significant effect on NTD when crossed to *Scrib*$^{rumz/+}$ embryos as no *Scrib*$^{rumz/+}$; *Vangl1*$^{KO/+}$ embryos exhibit NTD and only 4.8% of *Scrib*$^{rumz/+}$; *Vangl2*$^{KO/+}$ embryos display ONT. However, *Scrib*$^{rumz/+}$; *Vangl1*$^{KO/+}$*; Vangl2*$^{KO/+}$ triple heterozygotes do display a significant increase in NTDs with approximately 6% exhibiting ONT, although this is still significantly smaller than the percentage of *Scrib*$^{rumz/+}$*; Vangl2*$^{Lp/+}$ embryos (Figure 2B). Similar results were observed in *Scrib*$^{Crc/+}$; *Vangl1*$^{KO/+}$, *Scrib*$^{Crc/+}$; *Vangl2*$^{KO/+}$, and *Scrib*$^{Crc/+}$; *Vangl1*$^{KO/+}$*; Vangl2*$^{KO/+}$ embryos (data not shown). Additionally, phenotypes were further characterized as normal, kinked tail, developmental delay (E9-10) brain closure defect (open forebrain or hindbrain), abdominal wall defect (omphalocele), ONT (CRN), or ONT with axial torsion in order to compare the distribution of minor defects caused by *Scrib* and *Vangl2* genetic interactions (Supplemental Figure 2). Interestingly approximately 50% of *Scrib*$^{rumz/+}$; *Vangl1*$^{KO/+}$*; Vangl2*$^{KO/+}$ embryos displayed minor defects with abdominal wall defects and kink tails being most prominently observed with approximately 16% of embryos exhibiting each (Supplemental Figure 2). Furthermore, different abnormalities were apparent in *Scrib*$^{rumz/+}$*; Vangl2*$^{p/+}$ and *Scrib*$^{Crc/+}$*; Vangl2*$^{Lp/+}$ embryos where *Scrib*$^{rumz/+}$*; Vangl2*$^{Lp/+}$ embryos mostly display ONT and developmental delays while *Scrib*$^{Crc/+}$*; Vangl2*$^{Lp/+}$ embryos largely exhibit turning defects and kinked tails (Supplemental Figure 2). To observe Vangl2 localization when *Scrib* is mutated we utilized the Vangl2$^{GFP/GFP}$ transgenic mouse line which contains GFP labelled endogenous Vangl2. Embryos from *Scrib*$^{rumz/+}$*; Vangl2*$^{GFP/+}$ double heterozygote crosses were dissected and fixed at E8.5 and the neural tissue was imaged (Figure 2C). Vangl2

was similarly localized to the cell membrane in wildtype, *Scrib*$^{rumz/+}$ and Scrib$^{rumz/rumz}$ embryos (Figure 2C), suggesting that Scrib and Vangl2 protein interactions are intact in *Scrib*^{rumz} embryos. These results in *Scrib*^{rumz} tissue are different from previously published data in *Scrib*^{Crc} mice lacking Scrib expression where Vangl2 localization is increased at the apical membrane in *Scrib*$^{Crc/Crc}$ neural tissue (Kharfallah et al., 2017).

Overall, these data are consistent with previous studies showing that *Scrib* genetically interacts with *Vangl2*^{Lp} (Murdoch et al., 2001b, Zarbalis et al., 2004), however they highlight that the genetic interaction with *Vangl2*^{Lp} is not solely due to lack of interaction between Scrib and Vangl proteins but must be due to additional interactions between Scrib and some other protein(s) that are affected by the *Vangl2*^{Lp} mutation. Not only are the phenotypes that result from genetic interactions of *Scrib*$^{rumz/+}$ and *Vangl2*$^{KO/+}$ less severe, but the additional loss of one allele of *Vangl1* in *Scrib*$^{rumz/+}$; *Vangl1*$^{KO/+}$; *Vangl2*$^{KO/+}$ embryos does not phenocopy the genetic interaction with *Vangl2*^{Lp}. In addition, the types of defects seen in triple heterozygotes *Scrib*$^{rumz/+}$; *Vangl1*$^{KO/+}$; *Vangl2*$^{KO/+}$ are qualitatively different from those seen in *Scrib*$^{rumz/+}$; *Vangl2*$^{Lp/+}$ embryos (Supplemental Figure 2).

Scrib affects CE of the neural tube.

To determine whether the NTD observed in *Scrib* mutants could be attributed to inhibition of convergent extension (CE), we crossed *Scrib*^{rumz} mice with the *mT/mG* line, and used fluorescently labeled E8.0 (1-3 somites) embryos in live confocal imaging for 6-10 hours to visualize tissue shape changes and overall elongation during NTC. Distortion diagrams drawn from relative cell positions tracked over time were used to quantify CE of the neural plate. In wildtype and *Scrib*$^{rumz/+}$ heterozygote movies the tissue elongates and narrows over time, while *Scrib*$^{rumz/rumz}$ mutant tissue underwent less CE (Supplemental movies 1-3). The overall change in CE index per hour in wildtype and *Scrib*$^{rumz/+}$ embryo movies is approximately 2% and 1.5% compared to -0.7% in *Scrib*$^{rumz/rumz}$ embryo movies (Figure 3A). When broken down to axial components, we found no significant difference in the amount of elongation between the genotypes, but observed a difference in the amount of convergence (Figure 3B). The wildtype neural

plate narrows significantly by 2.7% per hour while the *Scrib*$^{rumz/rumz}$ neural plate widens by 1.5% per hour. The *Scrib*$^{rumz/+}$ neural plate does narrow although to a lesser degree, by 1.0% per hour (Figure 3B). The number of cells within the distortion diagram area remain the same at the start and end of the movies in wildtype, *Scrib*$^{rumz/+}$, and *Scrib*$^{rumz/rumz}$ (Supplemental Figure 3A), while the overall area of the designated distortion diagram decreases as the movies progress in wildtype but increases in *Scrib*$^{rumz/+}$ and *Scrib*$^{rumz/rumz}$ movies (Supplemental Figure 3B). These results suggest that changes in tissue shape and lack of CE are not due to changes in proliferation or cell number but instead due to differences in cell intercalation and cell shape. With these live imaging experiments, we identified a novel role for Scrib in regulating CE during mammalian neural tube development.

Scrib regulates mechanisms of cell rearrangement and polarity of intercalation.

CE results from cells intercalating mediolaterally to extend the tissue in the AP direction (Keller, 2002, Keller and Sutherland, 2020, Sutherland et al., 2020), and we have shown previously that defects in the polarity or frequency of cell intercalation lead to decreased CE (Williams et al., 2014). The frequency and polarity of cell intercalation in embryos from *Scrib*$^{rumz/+}$ heterozygote crosses were assessed by live imaging. Cells were tracked throughout the movies of *mT/mG* fluorescently labeled E8.0 (1-3 somites) described above, and for each embryo, rearrangements were analyzed in several clusters of approximately 10 cells each. The rearrangements were classified as resulting from rosette resolution, T1 process, single cell intercalation, or from cell division (Williams et al., 2014). The polarity was determined by measuring the angle of separation of neighboring cells relative to the AP axis of the embryo, with the assumption that separation of neighboring cells along the AP axis results from a mediolateral intercalation, while a separation along the ML axis represents an AP intercalation. No significant differences in the total number of cell separations per cluster were observed between wildtype, *Scrib*$^{rumz/+}$ and *Scrib*$^{rumz/rumz}$ embryos (Figure 3C). The relative frequency of the various types of cell rearrangements was similar between wildtype, *Scrib*$^{rumz/+}$ and *Scrib*$^{rumz/rumz}$ embryos (Figure 3D). However, we observed distinct effects of the *Scrib*^{rumz}

mutation on the process of rosette resolution, with many rosettes forming and then resolving back in the original direction, and others forming, resolving, and then reforming. To characterize rosette formation and resolution in more depth, all rosettes observed were classified as either not resolved (a rosette formed and remained in the rosette configuration until the end of the movie), resolved by junctional rearrangement (a rosette forms and coordinated junctional rearrangement leads to neighbor exchange), or resolved by division (a rosette forms and division of cells within or near the rosette disrupts its configuration) (Figure 3G). We further classified the rosettes that resolved by junctional rearrangement into two groups: those in which the cells go from orientation along one axis to rosette formation and then resolve into orientation along the other axis (productive junctional rearrangement), and those in which the cells go from orientation along one axis to rosette formation and then resolve back along the original axis (unproductive junctional rearrangement) (Figure 3G). A final group, only observed in *Scrib*$^{rumz/+}$ *and Scrib*$^{rumz/rumz}$ embryos, were rosettes that repetitively formed and resolved (pulsing rosettes) (Figure 3G). These categories differed significantly between the three genotypes (Figure 3D): the frequency of productive junctional rearrangement went down in the *Scrib*$^{rumz/+}$ embryos, and was gone in the mutant, while the frequency of unproductive junctional rearrangements and pulsing rosettes went up in the *Scrib*$^{rumz/+}$ embryo, and increased further in the mutant. In addition, the specific polarity of formation and productive resolution of rosettes was strongly affected by the *Scrib*^{rumz} mutation. In wildtype embryos the majority of rosettes formed along the ML axis and resolved along the AP axis, whereas in *Scrib*$^{rumz/+}$ embryos there was an equal frequency of formation along the ML and AP axes and resolution along the other axis (Figure 3F). Additionally, no *Scrib*$^{rumz/rumz}$ rosettes resolved productively by junctional rearrangement with about 43% of rosette resolutions resulting in unproductive separations and the remaining resolutions taking place by division (Figure 3E). Importantly, none of the rosettes formed in *Scrib*$^{rumz/rumz}$ tissue led to a change in the orientation of the cell clusters emphasizing the lack of productivity of rosette intercalations in *Scrib*$^{rumz/rumz}$ embryos (Figure 3F).

Mutation of Scrib also had a strong effect on the polarity of cell intercalation. The majority of wildtype and *Scrib*$^{rumz/+}$ cells separations occured in the AP direction, indicating mediolaterally polarized intercalation, whereas *Scrib*$^{rumz/rumz}$ cells separations occurred

equally in all directions (Figure 4H). Together these data underline an important role for Scrib in determining the polarity of intercalation as well as in promoting rosette resolution and suggest that defects in polarized cell intercalation contribute to impaired tissue shape changes and CE in *Scrib*$^{rumz/rumz}$ embryos.

Scrib promotes apical constriction.

Cells must transform from columnar to wedge shape in order for the neural tube to bend (Inoue et al., 2016, McShane et al., 2015, Smith et al., 1994). Our previous data show that floorplate cells normally increase area and elongate basally along the mediolateral axis, while decreasing area (constricting) and remaining more rounded apically (Williams et al., 2014). We observed normal basal elongation and orientation of cells in wildtype and *Scrib*$^{rumz/+}$ embryos, however, the basal ends of neural cells in *Scrib*$^{rumz/rumz}$ embryos did not elongate, and their long axis was randomly oriented relative to the AP axis of the embryo (Figure 4A). Rose plots representing the orientation of the long axis of the basal ends of cells show predominant orientation along the ML axis (0-180º) in both wildtype and *Scrib*$^{rumz/+}$ embryos, whereas *Scrib*$^{rumz/rumz}$ cells are not oriented in a particular direction as shown by the uniform rose plot (Figure 4A). Cell wedging occurred in wildtype embryos as apical cell area decreased (Figure 4B), while the apical constriction index (ACI), ratio of basal cell area over apical cell area, increased (Figure 4C). Surprisingly, in *Scrib*$^{rumz/+}$ cells apical cell area increased and the ACI decreased suggesting that the apical end is not constricting but instead getting larger, and the cells are becoming more columnar (Figure 4B,C). Cell area in *Scrib*$^{rumz/rumz}$ neural cells does not change significantly at the apical end resulting in a decrease in ACI (Figure 4B,C). Thus *Scrib* mutants do not transform from columnar to wedge shaped cells as required for neural plate bending, suggesting a role for Scrib in regulating apical constriction during NTC. Furthermore, the decreased apical constriction in heterozygous embryos suggests that the mutation may have some dominant effects on this process.

Localization and expression of junctional proteins is affected by Scrib mutation.

Cell rearrangements and cell shape changes rely on cell-cell interactions, shortening of junctions, and formation of new junctions (Shindo, 2018, Rauzi et al., 2010). Given Scrib's role in maintaining junctional composition, mediating junctional remodeling, and regulating E-cadherin retention and recycling at the adherens junction (Bonello and Peifer, 2018, Lohia et al., 2012), it is possible that Scribble regulates CE and apical constriction by influencing the localization and expression of junctional proteins. Components of the Atypical Protein Kinase C (aPKC) complex, aPKC and Partitioning defective 6 (Par6) which are normally enriched at the apical surface and at tight junctions with lower expression in the cytoplasm are increased at the apical surface in *Scrib*$^{rumz/+}$ cells but decreased in *Scrib*$^{rumz/rumz}$ cells (Figure 5A,B). In contrast, localization of partitioning defective 3 (Par3), the third component of the aPKC apical polarity complex, is decreased in both *Scrib*$^{rumz/+}$ and *Scrib*$^{rumz/rumz}$ tissue compared to the wildtype neural plate (Figure 5A,B). The tight junction protein Zonula Occludin-1 (ZO-1) is decreased at junctions in both *Scrib*$^{rumz/+}$ and *Scrib*$^{rumz/rumz}$ cells as compared to wildtype, but expression is unchanged in the cytoplasm (Figure 5A,B). This suggests that ZO-1 expression is decreased at the junctions and not simply mislocalized into the cytoplasm. N-cadherin (N-cad) expression is decreased in the cytoplasm of *Scrib*$^{rumz/+}$ tissue and decreased in *Scrib*$^{rumz/rumz}$ tissue at both the junction and cytoplasm compared to wildtype while E-cadherin (E-cad) is decreased in both the cytoplasm and at the junction of *Scrib*$^{rumz/+}$ cells and further decreased in *Scrib*$^{rumz/rumz}$ tissue (Figure 5A,B).This suggests that cadherin membrane retention and degradation is affected by *Scrib* mutation in neural cells. Overall, *Scrib*^{rumz} affects the expression and localization of several apical and tight junction proteins including aPKC, Par3, and ZO-1 and disrupts retention of cadherin at the membrane confirming a role for Scrib in targeting proteins critical for cell interactions and junctional remodeling to the cell membrane during NTC.

Scrib regulates cytoskeletal proteins during NTC.

Junctional shrinkage and rearrangement depends on actin and myosin dynamics, organization, and anchorage to adherens junctions ((Bertet et al., 2004, Blankenship et al., 2006, Rauzi et al., 2010, Fernandez-Gonzalez and Zallen, 2011) and reviewed in

(Sutherland and Lesko, 2020, Heer and Martin, 2017)). Scrib is known to interact with several cytoskeleton-associated proteins such as βPIX, vimentin, and Lgl (Osmani et al., 2006, Phua et al., 2009, Raman et al., 2018), thus Scrib may play a role in regulating the linkage between the actomyosin network and the adherens junction in neural epithelial cells. Actin staining is very crisp at cell membranes in wildtype neural tissue and enriched at the apical surface; however, in *Scrib*$^{rumz/+}$ tissue actin localization at cell junctions is decreased significantly and is further decreased in *Scrib*$^{rumz/rumz}$ tissue compared to *Scrib*$^{rumz/+}$ cells (Figure 6A,B). Similarly, MIIB is decreased in both *Scrib*$^{rumz/+}$ and *Scrib*$^{rumz/rumz}$ tissue at cell junctions compared to wildtype cells (Figure 6A,B).Surprisingly, MIIA junctional expression is increased in *Scrib*$^{rumz/rumz}$ tissue compared to wildtype and *Scrib*$^{rumz/+}$ cells (Figure 6A,B). Disruption of both actin and myosin expression and localization in *Scrib*$^{rumz/rumz}$ mutants suggest that changes in actomyosin dynamics may be leading to the observed defects in junctional rearrangement and cell shape changes during NTC.

Discussion

NTD occur in 1:500 pregnancies (Blencowe et al., 2018) resulting in birth defects such as anencephaly, spina bifida, and CRN (depending on where the failure of NTC occurs) (Greene and Copp, 2014). Morphogenesis of the epithelial neural plate into the neural tube includes elongation and narrowing of the tissue through CE, and bending through apical constriction and cell wedging (McShane et al., 2015, Inoue et al., 2016, Keller, 2002, Sutherland et al., 2020, Keller and Sutherland, 2020). The PCP pathway has been shown to play a major role in orchestrating these events, as mutations in genes encoding PCP components lead to NTD (Wu et al., 2011, Greene and Copp, 2014, Zohn, 2020). Other proteins that affect PCP signaling similarly affect neural morphogenesis, and in particular, mutations in the gene encoding the protein Scrib cause NTD and interact genetically with mutations in Vangl2. However, the molecular and cellular mechanisms by which Scrib promotes NTC remain largely unknown. Here we have identified a role for Scrib in promoting both polarized cell intercalation during CE and cell shape changes that cause bending in the neural plate. Furthermore, we have shown that Scrib mutation

affects the composition of both tight and adherens junctions and the organization of the apical cytoskeleton. These studies clarify the role of Scribble in NTC and broadened our understanding of mammalian neural tube development.

Scrib and PCP pathway interactions

Previous studies have shown that mutations in *Scrib* genetically interact with *Vangl2*^{Lp} to cause CRN (Murdoch et al., 2001b, Zarbalis et al., 2004, Murdoch et al., 2014), which has been attributed to the direct interaction known to exist between Scrib and Vangl2 through the Scrib C-terminal PDZ domains (Kallay et al., 2006, Courbard et al., 2009, Montcouquiol et al., 2006, Belotti et al., 2013). Our observations of NTD in *Scrib*$^{rumz/+}$*; Vangl2*$^{Lp/+}$ and *Scrib*$^{Crc/+}$*; Vangl2*$^{Lp/+}$ are consistent with those previous results showing genetic interaction and identifying variable phenotypes in *Scrib*$^{Crc/+}$*; Vangl2*$^{Lp/+}$ embryos (Murdoch et al., 2014, Murdoch et al., 2001b, Zarbalis et al., 2004). However, by examining double heterozygotes of either *Scrib*$^{rumz/+}$ or *Scrib*$^{Crc/+}$ and *Vangl2*$^{KO/+}$ as well as, Vangl2 localization in *Scrib*^{rumz} tissue we show that the genetic interaction between *Scrib* mutants and *Vangl*^{Lp} is not simply due to heterozygosity for Scrib and Vangl2, as *Scrib*$^{rumz/+}$*; Vangl2*$^{KO/+}$ embryos have less severe, but qualitatively different phenotypes than *Scrib*$^{rumz/+}$*; Vangl2*$^{Lp/+}$ embryos. While in principle this could be attributed to compensation by Vangl1 given that Vangl1 and Vangl2 are very similar in structure and function (Murdoch et al., 2001a, Gravel et al., 2010, Iliescu et al., 2011, Torban et al., 2004), and that *Vangl2*^{Lp} has a dominant negative effect on *Vangl1* (Yin et al., 2012), our results do not support this interpretation. *Scrib*$^{rumz/+}$*; Vangl1*$^{KO/+}$ embryos do not exhibit ONT, and a similar percentage of *Scrib*$^{rumz/+}$*; Vangl2*$^{KO/+}$ double heterozygotes and *Scrib*$^{rumz/+}$*; Vangl1*$^{KO/+}$; *Vangl2*$^{KO/+}$ triple heterozygotes exhibit ONT. These observations suggest that the dominant effect of the *Vangl2*^{Lp} mutation may be affecting a different, unknown, component of the PCP signaling pathway, or alternatively, that *Vangl2*^{Lp} has a dominant negative effect on Scrib itself. The *Vangl2*^{Lp} mutation inhibits trafficking of Vangl2 to the cell membrane (Merte et al., 2010), and it is possible that through direct or indirect interactions Scrib is trapped in the cytoplasm by Vangl2 and therefore unable to complete necessary functions at the membrane for NTC.

Scrib affects polarized cell intercalation

Scrib$^{rumz/rumz}$ neural tissue overall exhibits somewhat decreased CE, and in particular, decreased narrowing (convergence). *Scrib*$^{rumz/rumz}$ mutants exhibit disrupted cell intercalation polarity, as well as a loss of the normal basal elongation and orientation of neural cells. Interestingly, this phenotype resembles that seen in embryos lacking Ptk7, but not that of *Vangl2*$^{Lp/Lp}$ mutants where decreased CE is due to decreased frequency of cell intercalations and not defects in polarized cell intercalation or basal cell orientation (Williams et al., 2014). The difference between *Scrib* and *Vangl2*^{Lp} mutants on CE and cell intercalation behavior suggest that they are not primarily regulating the same cellular processes during neural morphogenesis, and that the genetic interaction between these mutants may lie in complementary effects on cell behavior. Thus, the effects of Scrib on intercalation polarity may synergize with those of Vangl2^{Lp} on intercalation frequency. The similarities between *Scrib*$^{rumz/rumz}$ and *Ptk7*$^{XST87/XST87}$ embryos suggest that Scrib and Ptk7 may act on similar downstream effectors such as MIIB which is disorganized in *Ptk7*$^{XST87/XST87}$ mutant neural tissue or Rho Kinase (ROCK) which regulates cell shape changes needed for NTC in *Ptk7*$^{XST87/XST87}$ embryos (Williams et al., 2014, Ybot-Gonzalez et al., 2007). However, Scrib and Ptk7 likely act on these targets through parallel pathways as the *Scrib*^{Crc} mutation does not interact genetically with the *Ptk7*^{chuzhoi} mutant to cause NTD (Paudyal et al., 2010).

While the *Scrib*^{rumz} mutation does not significantly affect the frequency of different types of cell rearrangements, a key observation is the very distinct effects that it has on cell behavior in rosette formations. The loss of one normal allele not only leads to a randomization of the polarity of rosette formation and junctional resolution, such that rosettes will form from ML and resolve to AP equally as often as they form from AP and resolve to ML, but also leads to rosettes that form and then resolve back in the same direction (ML to ML or AP to AP). With the loss of two normal alleles, we observe that any junctional rearrangements of rosettes either lead to resolution back along the original axis, or to repetitive formation and resolution of rosettes of the same groups of cells, without any net change in the position of the cells. In addition, in mutant embryos we also observed numerous rosettes that formed and remained as rosettes for the rest of the

movie. Interestingly, we also observed these behaviors in *Vangl2^{Lp}* embryos, where the polarity of resolution was randomized, and many rosettes were observed to remain in rosette conformation without resolution (Williams et al., 2014). These results suggest that rosette resolution is critically dependent on Scrib and Vangl2 function.

Comparison of the *Scrib^{rumz}*, *Vangl2^{Lp}, and Ptk7^{Xst87}* phenotypes raises interesting questions about the role of cell intercalation as a force-producing process that actively promotes elongation of the body axis during the early period of neural tube formation in the mouse. All three of these mutants strongly affect either the frequency or polarity of cell intercalation, but only the *Ptk7$^{XST87/XST87}$* mutant significantly decreases the overall CE of the body axis during this period. This suggests that mediolateral cell intercalation may not be the sole, or even the primary driver of neural CE during this period, but may cooperate with other mechanisms. One likely mechanism is an extrinsically generated biomechanical force, either from amniotic fluid pressure (Imuta et al., 2014), or alternatively, from tissue strain generated by the formation and enlargement of the headfolds (Sutherland et al., 2020, Gavrilov and Lacy, 2013). Studies of germband elongation in *Drosophila* have shown that the tensile force generated by posterior midgut invagination drives tissue CE as well as orienting cell rearrangement (Collinet et al., 2015, Yu and Fernandez-Gonzalez, 2016, Lye et al., 2015), and that in the absence of posterior midgut invagination, cell intercalation is not sufficient to drive tissue elongation (Yu and Fernandez-Gonzalez, 2016, Collinet et al., 2015). Accordingly, in the *Scrib^{rumz}* and *Vangl2^{Lp}* neural plates normal extrinsic forces may be successfully promoting extension despite the changes in cell intercalation. In the *Ptk7$^{XST87/XST87}$* mutant the additional loss of mesodermal CE may further affect neural CE, or alternatively, the effects on actin and myosin organization (Williams et al., 2014, Andreeva et al., 2014), may be changing the compliance of the tissue and affecting its response to normal extrinsic forces, leading to significantly decreased neural CE.

Junctional Integrity

Apical constriction and rosette resolution are disrupted in *Scrib$^{rumz/rumz}$* mutant cells, effects which may be due to changes in apical junctional integrity. ZO-1, aPKC,

Par6, Par3, E-cad, and N-cad expression and localization are decreased in the neural plate of *Scrib*$^{rumz/rumz}$ mutants. This is consistent with results of Scrib deletion in the head ectoderm of mouse embryos, which led to decreased E-cad and ZO-1 expression and aberrant cell shape changes in the cornea (Yamben et al., 2013), as well as, with a model of Scrib regulation of junctional integrity established in Madin Darby Canine Kidney (MDCK) cells (Yamanaka et al., 2003). In this model, loss of Scrib frees up Lethal giant larvae (Lgl), a polarity protein in the basal Scrib-Discs large (Dlg)-Lgl complex, to bind to aPKC and Par6 creating competition between Lgl and Par3 and subsequently inhibiting the formation of tight junctions (Yamanaka et al., 2003). In the neural plate, the *Scrib*^{rumz} mutation may disrupt interaction of Lgl with the Scrib LRR domain (Kallay et al., 2006, Abedrabbo and Ravid, 2020) allowing Lgl to localize to the apical membrane and bind to aPKC and Par6. The formation of an Lgl-aPKC-Par6 complex would displace Par3 from the complex and destabilize tight junctions leading to loss of ZO-1 and Par3 expression which is what we observe in *Scrib*$^{rumz/rumz}$ mutants. Additionally, this competition of Lgl would displace Par6 and aPKC from the apical junctions consistent with our observation that Par6 and aPKC apical expression is decreased in *Scrib*$^{rumz/rumz}$ cells. Increased apical expression of Par6 and aPKC in *Scrib*$^{rumz/+}$ tissue compared to wildtype can be explained by two distinct pools of Par6 and aPKC one binding the increased free Lgl (Lgl-Par6-aPKC) promoted by the mutation of one copy of Scrib, and the other binding Par3 (Par3-aPKC-Par6). Moreover, Scrib is important for retention and recycling of cadherin turnover at the junctions (Lohia et al., 2012); therefore, loss of Scrib would result in higher turnover and degradation of cadherin which we observed as decreased junctional expression of E-cad and N-cad through whole mount staining.

Actomyosin Pulsing and Biomechanics

Anchoring of the cytoskeleton to the junction is dependent on the presence of cadherins (Martin and Goldstein, 2014, Martin et al., 2010, Jodoin et al., 2015, Sawyer et al., 2011). Whole mount staining revealed that actin and MIIB are decreased while MIIA is increased at neural cell junctions in *Scrib*$^{rumz/rumz}$ mutant embryos. The decreased expression of actin and MIIB could be due to disrupted junctional integrity and loss of

cadherins, leading to unstable anchorage of the apical cytoskeleton to the junctions. Additionally, it could suggest slower turnover or higher degradation of actin and MIIB at junctions. Increased junctional expression of MIIA was surprising as MIIB and MIIA are often thought to have distinct cellular functions, and typically are not upregulated in response to loss of one or another isoform (Wang et al., 2010). However, MIIA is able to compensate for the loss of MIIB to maintain cell-cell adhesion in neural epithelial tissue (Ma and Adelstein, 2014, Wang et al., 2010)-. Therefore, it is possible that MIIA is increased in the *Scrib*$^{rumz/rumz}$ neural plate to help maintain cellular interactions in the absence of MIIB at cellular junctions. However, MIIA and MIIB are known to have different kinetic profiles (Kovács et al., 2003), and thus the change from MIIB to MIIA might alter cell intercalation behavior while preserving cell-cell adhesion. Alternatively, recent studies in human breast cancer cell lines demonstrated that MIIA co-immunoprecipitated with Lgl but not Scrib, and MIIB complexed with Scrib but not Lgl, demonstrating MIIA and MIIB form distinct complexes with Lgl and Scrib respectively (Abedrabbo and Ravid, 2020). Thus, the increase in MIIA we observe in the neural plate of *Scrib*^{rumz} mutants may be linked to increased Lgl at the apical membrane and the decreased expression of MIIB we found in the neural tissue of *Scrib*^{rumz} mutants may be due to lack of Scrib expression and localization at cell junctions. Future studies using live imaging of actin and myosin in the neural plate would be helpful to elucidate these dynamics.

Defects in expression and localization of actin and myosin suggest actomyosin contractions may be disrupted upon *Scrib* mutation. Actomyosin pulsing has been shown to be important for CE and apical constriction during embryonic development (Sutherland and Lesko, 2020, Murrell et al., 2015, Coravos et al., 2017, Heer and Martin, 2017). Although it has yet to be demonstrated in mouse neural tube, it is known that actin turnover and stabilization are important for pulsing forces during *Drosophila* embryo development (Jodoin et al., 2015, Dehapiot et al., 2020). Additionally, junctional remodeling is needed to promote a ratchet mechanism for pulsing where contractions promote junctional shrinkage and rearrangement (Rauzi et al., 2010). Our results suggest that turnover and/or junctional integrity may be disrupted in *Scrib*$^{rumz/rumz}$ mutants, suggesting that altered actomyosin pulsing is a possible mechanism for the defects in cell shape changed and cell behavior caused by the Scrib mutation. Actomyosin pulsing

contractions rely on a Rho-mediated mechanism (Michaux and Robin, 2018, Mason et al., 2016, Munjal et al., 2015, Garcia De Las Bayonas et al., 2019, Reyes et al., 2014, Bement et al., 2015, Dehapiot et al., 2020), which has been demonstrated to be disrupted in *Ptk7*$^{XST87XST87-}$ mutants with neural cell behavior defects that closely resemble the CE and apical constriction phenotypes we observed in *Scrib*$^{rumz/rumz}$ mutant embryos (Williams et al., 2014, Andreeva et al., 2014). Further studies focused on the role of Scrib in regulating Rho-mediated actomyosin pulsing warrant future investigation in order to better understand the genesis of the CE and apical constriction defects observed in *Scrib*$^{rumz/rumz}$ mutants.

Not only did we observe ONT in *Scrib*$^{rumz/rumz}$ mutant embryos but we also found prominent turning defects where mutant embryos exhibited axial torsion and, in some cases, a complete lack of turning. Mouse embryos usually turn on axis at around 10-12 somites, however how this process occurs is not fully understood. Turning defects in *Scrib*$^{rumz/rumz}$ mutants could be caused by the lack of CE resulting in a wider flatter neural plate as NTC progresses inhibiting tension and forces needed to initiate turning. Another possibility is that disrupted apical constriction in *Scrib*$^{rumz/rumz}$ embryos does not allow bending of the neural tube which may alleviate stress on the tissue, which is normally necessary for the embryo to turn. Finally, junctional composition, cytoskeleton organization, and actomyosin pulsing are required for biomechanical sensing and force propagation (Galea et al., 2017, Sutherland and Lesko, 2020, Coravos et al., 2017, Heer and Martin, 2017, Tharp and Weaver, 2018). We have shown disruption in junctional stability and cytoskeletal organization in *Scrib*$^{rumz/rumz}$ neural cells suggesting these processes may be required for the sensing of tension and force necessary for embryos to turn. Further studies are needed to determine whether this mechanism is at work in neural morphogenesis.

Conclusions

Here we investigate the effect of *Scrib* mutation on NTC and determine details of neural cell behavior regulated by Scrib. We show that *Scrib* mutants exhibit ONT and turning defects and genetically interact with *Vangl2*^{Lp} mutation to cause NTD. CE, specifically

narrowing, is disrupted in *Scrib*$^{rumz/rumz}$ mutant embryos, as well as, polarity of cell intercalations and resolution of rosettes as a mechanism of cell rearrangement. Apical constriction and cell shape changes are also disrupted in *Scrib*$^{rumz/rumz}$ mutants and we identified a role for Scrib in regulating junctional composition and cytoskeletal organization in the neural plate. Together these studies identify a novel role for Scrib in regulating neural cell behavior and provide a better understanding of NTC in mammalian development

Acknowledgements

We acknowledge the Keck Center for Cellular Imaging for the usage of the Zeiss 780 microscopy system (PI: AP; NIH-ODO16446) and the Leica SP5X microscopy system (PI:AP; NIH-RR025616). We also thank Dr. Xiaowei Lu for her helpful discussions and comments.

Funding Sources

This research was supported by the Eunice Kennedy Shriver National Institute of Child Health and Human Development-R01HD087093.

ABEDRABBO, M. & RAVID, S. 2020. Scribble, Lgl1, and myosin II form a complex in vivo to promote directed cell migration. *Mol Biol Cell*, mbcE19110657.

ANDREEVA, A., LEE, J., LOHIA, M., WU, X., MACARA, I. G. & LU, X. 2014. PTK7-Src signaling at epithelial cell contacts mediates spatial organization of actomyosin and planar cell polarity. *Dev Cell,* 29**,** 20-33.

AXELROD, J. D. & MCNEILL, H. 2002. Coupling planar cell polarity signaling to morphogenesis. *ScientificWorldJournal,* 2**,** 434-54.

BELOTTI, E., POLANOWSKA, J., DAULAT, A. M., AUDEBERT, S., THOMÉ, V., LISSITZKY, J. C., LEMBO, F., BLIBEK, K., OMI, S., LENFANT, N., GANGAR, A., MONTCOUQUIOL, M., SANTONI, M. J., SEBBAGH, M., AURRAND-LIONS, M., ANGERS, S., KODJABACHIAN, L., REBOUL, J. & BORG, J. P. 2013. The human PDZome: a gateway to PSD95-Disc large-zonula occludens (PDZ)-mediated functions. *Mol Cell Proteomics,* 12**,** 2587-603.

BEMENT, W. M., LEDA, M., MOE, A. M., KITA, A. M., LARSON, M. E., GOLDING, A. E., PFEUTI, C., SU, K. C., MILLER, A. L., GORYACHEV, A. B. & VON DASSOW, G. 2015. Activator-inhibitor coupling between Rho signalling and actin assembly makes the cell cortex an excitable medium. *Nat Cell Biol,* 17**,** 1471-83.

BERTET, C., SULAK, L. & LECUIT, T. 2004. Myosin-dependent junction remodelling controls planar cell intercalation and axis elongation. *Nature,* 429**,** 667-71.

BLANKENSHIP, J. T., BACKOVIC, S. T., SANNY, J. S., WEITZ, O. & ZALLEN, J. A. 2006. Multicellular rosette formation links planar cell polarity to tissue morphogenesis. *Dev Cell,* 11**,** 459-70.

BLENCOWE, H., KANCHERLA, V., MOORTHIE, S., DARLISON, M. W. & MODELL, B. 2018. Estimates of global and regional prevalence of neural tube defects for 2015: a systematic analysis. *Ann N Y Acad Sci,* 1414**,** 31-46.

BONELLO, T. T. & PEIFER, M. 2018. Scribble: A master scaffold in polarity, adhesion, synaptogenesis, and proliferation.

BUTLER, M. B., SHORT, N. E., MANIOU, E., ALEXANDRE, P., GREENE, N. D. E., COPP, A. J. & GALEA, G. L. 2019. Rho kinase-dependent apical constriction counteracts M-phase apical expansion to enable mouse neural tube closure. 132.

CHANG, H., SMALLWOOD, P. M., WILLIAMS, J. & NATHANS, J. 2016. The spatio-temporal domains of Frizzled6 action in planar polarity control of hair follicle orientation. *Dev Biol,* 409**,** 181-193.

COLLINET, C., RAUZI, M., LENNE, P. F. & LECUIT, T. 2015. Local and tissue-scale forces drive oriented junction growth during tissue extension. *Nat Cell Biol,* 17**,** 1247-58.

COPP, A. J. & GREENE, N. D. 2010. Genetics and development of neural tube defects. *J Pathol,* 220**,** 217-30.

COPP, A. J. & GREENE, N. D. 2013. Neural tube defects--disorders of neurulation and related embryonic processes. *Wiley Interdiscip Rev Dev Biol,* 2**,** 213-27.

CORAVOS, J. S., MASON, F. M. & MARTIN, A. C. 2017. Actomyosin Pulsing in Tissue Integrity Maintenance during Morphogenesis. *Trends Cell Biol,* 27**,** 276-283.

COURBARD, J. R., DJIANE, A., WU, J. & MLODZIK, M. 2009. The apical/basal-polarity determinant Scribble cooperates with the PCP core factor Stbm/Vang and functions as one of its effectors. *Dev Biol,* 333**,** 67-77.

DEHAPIOT, B., CLÉMENT, R., ALÉGOT, H., GAZSÓ-GERHÁT, G., PHILIPPE, J. M. & LECUIT, T. 2020. Assembly of a persistent apical actin network by the formin Frl/Fmnl tunes epithelial cell deformability. *Nat Cell Biol*.

DOW, L. E., KAUFFMAN, J. S., CADDY, J., ZARBALIS, K., PETERSON, A. S., JANE, S. M., RUSSELL, S. M. & HUMBERT, P. O. 2007. The tumour-suppressor Scribble dictates cell polarity during directed epithelial migration: regulation of Rho GTPase recruitment to the leading edge. *Oncogene,* 26**,** 2272-82.

ESCUIN, S., VERNAY, B., SAVERY, D., GURNIAK, C. B., WITKE, W., GREENE, N. D. & COPP, A. J. 2015. Rho-kinase-dependent actin turnover and actomyosin disassembly are necessary for mouse spinal neural tube closure. *J Cell Sci,* 128**,** 2468-81.

FERNANDEZ-GONZALEZ, R. & ZALLEN, J. A. 2011. Oscillatory behaviors and hierarchical assembly of contractile structures in intercalating cells. *Phys Biol,* 8**,** 045005.

GALEA, G. L., CHO, Y. J., GALEA, G., MOLE, M. A. & ROLO, A. 2017. Biomechanical coupling facilitates spinal neural tube closure in mouse embryos. 114**,** E5177-e5186.

GALEA, G. L., NYCHYK, O., MOLE, M. A., MOULDING, D., SAVERY, D., NIKOLOPOULOU, E., HENDERSON, D. J., GREENE, N. D. E. & COPP, A. J. 2018. Vangl2 disruption alters the biomechanics of late spinal neurulation leading to spina bifida in mouse embryos. *Dis Model Mech,* 11.

GARCIA DE LAS BAYONAS, A., PHILIPPE, J. M., LELLOUCH, A. C. & LECUIT, T. 2019. Distinct RhoGEFs Activate Apical and Junctional Contractility under Control of G Proteins during Epithelial Morphogenesis. *Curr Biol*.

GAVRILOV, S. & LACY, E. 2013. Genetic dissection of ventral folding morphogenesis in mouse: embryonic visceral endoderm-supplied BMP2 positions head and heart. *Curr Opin Genet Dev,* 23**,** 461-9.

GRAVEL, M., ILIESCU, A., HORTH, C., APUZZO, S. & GROS, P. 2010. Molecular and cellular mechanisms underlying neural tube defects in the loop-tail mutant mouse. *Biochemistry,* 49**,** 3445-55.

GREENE, N. D. & COPP, A. J. 2014. Neural tube defects. *Annu Rev Neurosci,* 37**,** 221-42.

HAMBLET, N. S., LIJAM, N., RUIZ-LOZANO, P., WANG, J., YANG, Y., LUO, Z., MEI, L., CHIEN, K. R., SUSSMAN, D. J. & WYNSHAW-BORIS, A. 2002. Dishevelled 2 is essential for cardiac outflow tract development, somite segmentation and neural tube closure. *Development,* 129**,** 5827-38.

HEER, N. C. & MARTIN, A. C. 2017. Tension, contraction and tissue morphogenesis. 144**,** 4249-4260.

HEISENBERG, C. P., TADA, M., RAUCH, G. J., SAUDE, L., CONCHA, M. L., GEISLER, R., STEMPLE, D. L., SMITH, J. C. & WILSON, S. W. 2000. Silberblick/Wnt11 mediates convergent extension movements during zebrafish gastrulation. *Nature,* 405**,** 76-81.

ILIESCU, A., GRAVEL, M., HORTH, C., APUZZO, S. & GROS, P. 2011. Transmembrane topology of mammalian planar cell polarity protein Vangl1. *Biochemistry,* 50**,** 2274-82.

IMUTA, Y., KOYAMA, H., SHI, D., EIRAKU, M., FUJIMORI, T. & SASAKI, H. 2014. Mechanical control of notochord morphogenesis by extra-embryonic tissues in mouse embryos. *Mech Dev,* 132**,** 44-58.

INOUE, Y., SUZUKI, M., WATANABE, T., YASUE, N., TATEO, I., ADACHI, T. & UENO, N. 2016. Mechanical roles of apical constriction, cell elongation, and cell migration during neural tube formation in Xenopus. *Biomech Model Mechanobiol,* 15**,** 1733-1746.

JODOIN, J. N., CORAVOS, J. S., CHANET, S., VASQUEZ, C. G., TWOROGER, M., KINGSTON, E. R., PERKINS, L. A., PERRIMON, N. & MARTIN, A. C. 2015. Stable Force Balance between Epithelial Cells Arises from F-Actin Turnover. *Dev Cell,* 35**,** 685-97.

KALLAY, L. M., MCNICKLE, A., BRENNWALD, P. J., HUBBARD, A. L. & BRAITERMAN, L. T. 2006. Scribble associates with two polarity proteins, Lgl2 and Vangl2, via distinct molecular domains. *J Cell Biochem,* 99**,** 647-64.

KELLER, R. 2002. Shaping the vertebrate body plan by polarized embryonic cell movements. *Science,* 298**,** 1950-4.

KELLER, R. & SUTHERLAND, A. 2020. Convergent extension in the amphibian, Xenopus laevis. *Curr Top Dev Biol,* 136**,** 271-317.

KHARFALLAH, F., GUYOT, M. C., EL HASSAN, A. R., ALLACHE, R., MERELLO, E., DE MARCO, P., DI CRISTO, G., CAPRA, V. & KIBAR, Z. 2017. Scribble1 plays an important role in the pathogenesis of neural tube defects through its mediating effect of Par-3 and Vangl1/2 localization. *Hum Mol Genet,* 26**,** 2307-2320.

KIBAR, Z., VOGAN, K. J., GROULX, N., JUSTICE, M. J., UNDERHILL, D. A. & GROS, P. 2001. Ltap, a mammalian homolog of Drosophila Strabismus/Van Gogh, is altered in the mouse neural tube mutant Loop-tail. *Nat Genet,* 28**,** 251-5.

KINOSHITA, N., SASAI, N., MISAKI, K. & YONEMURA, S. 2008. Apical accumulation of Rho in the neural plate is important for neural plate cell shape change and neural tube formation. *Mol Biol Cell,* 19**,** 2289-99.

KOVÁCS, M., WANG, F., HU, A., ZHANG, Y. & SELLERS, J. R. 2003. Functional divergence of human cytoplasmic myosin II: kinetic characterization of the non-muscle IIA isoform. *J Biol Chem,* 278**,** 38132-40.

LEI, Y., ZHU, H., DUHON, C., YANG, W., ROSS, M. E., SHAW, G. M. & FINNELL, R. H. 2013. Mutations in planar cell polarity gene SCRIB are associated with spina bifida. *PLoS One,* 8**,** e69262.

LOHIA, M., QIN, Y. & MACARA, I. G. 2012. The Scribble polarity protein stabilizes E-cadherin/p120-catenin binding and blocks retrieval of E-cadherin to the Golgi. *PLoS One,* 7**,** e51130.

LÓPEZ-ESCOBAR, B., CARO-VEGA, J. M., VIJAYRAGHAVAN, D. S., PLAGEMAN, T. F., SANCHEZ-ALCAZAR, J. A., MORENO, R. C., SAVERY, D., MÁRQUEZ-RIVAS, J., DAVIDSON, L. A. & YBOT-GONZÁLEZ, P. 2018. The non-canonical Wnt-PCP pathway shapes the mouse caudal neural plate. *Development,* 145.

LYE, C. M., BLANCHARD, G. B., NAYLOR, H. W., MURESAN, L., HUISKEN, J., ADAMS, R. J. & SANSON, B. 2015. Mechanical Coupling between Endoderm Invagination and Axis Extension in Drosophila. *PLoS Biol,* 13**,** e1002292.

MA, X. & ADELSTEIN, R. S. 2014. The role of vertebrate nonmuscle Myosin II in development and human disease. *Bioarchitecture,* 4**,** 88-102.

MARTIN, A. C., GELBART, M., FERNANDEZ-GONZALEZ, R., KASCHUBE, M. & WIESCHAUS, E. F. 2010. Integration of contractile forces during tissue invagination. *J Cell Biol,* 188**,** 735-49.

MARTIN, A. C. & GOLDSTEIN, B. 2014. Apical constriction: themes and variations on a cellular mechanism driving morphogenesis. *Development,* 141**,** 1987-98.

MASON, F. M., XIE, S., VASQUEZ, C. G., TWOROGER, M. & MARTIN, A. C. 2016. RhoA GTPase inhibition organizes contraction during epithelial morphogenesis. *J Cell Biol,* 214**,** 603-17.

MCSHANE, S. G., MOLE, M. A., SAVERY, D., GREENE, N. D., TAM, P. P. & COPP, A. J. 2015. Cellular basis of neuroepithelial bending during mouse spinal neural tube closure. *Dev Biol,* 404**,** 113-24.

MERTE, J., JENSEN, D., WRIGHT, K., SARSFIELD, S., WANG, Y., SCHEKMAN, R. & GINTY, D. D. 2010. Sec24b selectively sorts Vangl2 to regulate planar cell polarity during neural tube closure. *Nat Cell Biol,* 12**,** 41-6; sup pp 1-8.

MICHAUX, J. B. & ROBIN, F. B. 2018. Excitable RhoA dynamics drive pulsed contractions in the early C. elegans embryo. 217**,** 4230-4252.

MONTCOUQUIOL, M., SANS, N., HUSS, D., KACH, J., DICKMAN, J. D., FORGE, A., RACHEL, R. A., COPELAND, N. G., JENKINS, N. A., BOGANI, D., MURDOCH, J., WARCHOL, M. E., WENTHOLD, R. J. & KELLEY, M. W. 2006. Asymmetric localization of Vangl2 and Fz3 indicate novel mechanisms for planar cell polarity in mammals. *J Neurosci,* 26**,** 5265-75.

MOURY, J. D. & SCHOENWOLF, G. C. 1995. Cooperative model of epithelial shaping and bending during avian neurulation: autonomous movements of the neural plate, autonomous movements of the epidermis, and interactions in the neural plate/epidermis transition zone. *Dev Dyn,* 204**,** 323-37.

MUNJAL, A., PHILIPPE, J. M., MUNRO, E. & LECUIT, T. 2015. A self-organized biomechanical network drives shape changes during tissue morphogenesis. *Nature,* 524**,** 351-5.

MUNRO, E. M. & ODELL, G. M. 2002. Polarized basolateral cell motility underlies invagination and convergent extension of the ascidian notochord. *Development,* 129**,** 13-24.

MURDOCH, J. N., DAMRAU, C., PAUDYAL, A., BOGANI, D., WELLS, S., GREENE, N. D., STANIER, P. & COPP, A. J. 2014. Genetic interactions between planar cell polarity genes cause diverse neural tube defects in mice. *Dis Model Mech,* 7**,** 1153-63.

MURDOCH, J. N., DOUDNEY, K., PATERNOTTE, C., COPP, A. J. & STANIER, P. 2001a. Severe neural tube defects in the loop-tail mouse result from mutation of Lpp1, a novel gene involved in floor plate specification. *Hum Mol Genet,* 10**,** 2593-601.

MURDOCH, J. N., HENDERSON, D. J., DOUDNEY, K., GASTON-MASSUET, C., PHILLIPS, H. M., PATERNOTTE, C., ARKELL, R., STANIER, P. & COPP, A. J. 2003. Disruption of scribble (Scrb1) causes severe neural tube defects in the circletail mouse. *Hum Mol Genet,* 12**,** 87-98.

MURDOCH, J. N., RACHEL, R. A., SHAH, S., BEERMANN, F., STANIER, P., MASON, C. A. & COPP, A. J. 2001b. Circletail, a new mouse mutant with severe neural tube defects: chromosomal localization and interaction with the loop-tail mutation. *Genomics,* 78**,** 55-63.

MURRELL, M., OAKES, P. W., LENZ, M. & GARDEL, M. L. 2015. Forcing cells into shape: the mechanics of actomyosin contractility. *Nat Rev Mol Cell Biol,* 16**,** 486-98.

MUZUMDAR, M. D., TASIC, B., MIYAMICHI, K., LI, L. & LUO, L. 2007. A global double-fluorescent Cre reporter mouse. *Genesis,* 45**,** 593-605.

NIKOLOPOULOU, E., GALEA, G. L., ROLO, A., GREENE, N. D. & COPP, A. J. 2017. Neural tube closure: cellular, molecular and biomechanical mechanisms. *Development,* 144**,** 552-566.

OSMANI, N., VITALE, N., BORG, J. P. & ETIENNE-MANNEVILLE, S. 2006. Scrib controls Cdc42 localization and activity to promote cell polarization during astrocyte migration. *Curr Biol,* 16**,** 2395-405.

PAUDYAL, A., DAMRAU, C., PATTERSON, V. L., ERMAKOV, A., FORMSTONE, C., LALANNE, Z., WELLS, S., LU, X., NORRIS, D. P., DEAN, C. H., HENDERSON, D. J. & MURDOCH, J. N. 2010. The novel mouse mutant, chuzhoi, has disruption of Ptk7 protein and exhibits defects in neural tube, heart and lung development and abnormal planar cell polarity in the ear. *BMC Dev Biol,* 10**,** 87.

PHUA, D. C., HUMBERT, P. O. & HUNZIKER, W. 2009. Vimentin regulates scribble activity by protecting it from proteasomal degradation. *Mol Biol Cell,* 20**,** 2841-55.

QIAN, D., JONES, C., RZADZINSKA, A., MARK, S., ZHANG, X., STEEL, K. P., DAI, X. & CHEN, P. 2007. Wnt5a functions in planar cell polarity regulation in mice. *Dev Biol,* 306**,** 121-33.

RAMAN, R., PINTO, C. S. & SONAWANE, M. 2018. Polarized Organization of the Cytoskeleton: Regulation by Cell Polarity Proteins. *J Mol Biol,* 430**,** 3565-3584.

RAUZI, M., LENNE, P. F. & LECUIT, T. 2010. Planar polarized actomyosin contractile flows control epithelial junction remodelling. *Nature,* 468**,** 1110-4.

REYES, C. C., JIN, M., BREZNAU, E. B., ESPINO, R., DELGADO-GONZALO, R., GORYACHEV, A. B. & MILLER, A. L. 2014. Anillin regulates cell-cell junction integrity by organizing junctional accumulation of Rho-GTP and actomyosin. *Curr Biol,* 24**,** 1263-70.

ROBINSON, A., ESCUIN, S., DOUDNEY, K., VEKEMANS, M., STEVENSON, R. E., GREENE, N. D., COPP, A. J. & STANIER, P. 2012. Mutations in the planar cell polarity genes CELSR1 and SCRIB are associated with the severe neural tube defect craniorachischisis. *Hum Mutat,* 33**,** 440-7.

SADLER, T. W. 2005. Embryology of neural tube development. *Am J Med Genet C Semin Med Genet,* 135c**,** 2-8.

SAWYER, J. K., CHOI, W., JUNG, K. C., HE, L., HARRIS, N. J. & PEIFER, M. 2011. A contractile actomyosin network linked to adherens junctions by Canoe/afadin helps drive convergent extension. *Mol Biol Cell,* 22**,** 2491-508.

SHINDO, A. 2018. Models of convergent extension during morphogenesis. *Wiley Interdiscip Rev Dev Biol,* 7.

SMITH, J. L., SCHOENWOLF, G. C. & QUAN, J. 1994. Quantitative analyses of neuroepithelial cell shapes during bending of the mouse neural plate. *J Comp Neurol,* 342**,** 144-51.

SONG, H., HU, J., CHEN, W., ELLIOTT, G., ANDRE, P., GAO, B. & YANG, Y. 2010. Planar cell polarity breaks bilateral symmetry by controlling ciliary positioning. *Nature,* 466**,** 378-82.

SUN, Z. & AMOURDA, C. 2017. Basolateral protrusion and apical contraction cooperatively drive Drosophila germ-band extension. 19**,** 375-383.

SUTHERLAND, A., KELLER, R. & LESKO, A. 2020. Convergent extension in mammalian morphogenesis. *Semin Cell Dev Biol,* 100**,** 199-211.

SUTHERLAND, A. & LESKO, A. 2020. Pulsed actomyosin contractions in morphogenesis. *F1000 Research,* 9.

SUZUKI, M., MORITA, H. & UENO, N. 2012. Molecular mechanisms of cell shape changes that contribute to vertebrate neural tube closure. *Dev Growth Differ,* 54**,** 266-76.

TADA, M. & SMITH, J. C. 2000. Xwnt11 is a target of Xenopus Brachyury: regulation of gastrulation movements via Dishevelled, but not through the canonical Wnt pathway. *Development,* 127**,** 2227-38.

THARP, K. M. & WEAVER, V. M. 2018. Modeling Tissue Polarity in Context. *J Mol Biol,* 430**,** 3613-3628.

TORBAN, E., WANG, H. J., GROULX, N. & GROS, P. 2004. Independent mutations in mouse Vangl2 that cause neural tube defects in looptail mice impair interaction with members of the Dishevelled family. *J Biol Chem,* 279**,** 52703-13.

WALLINGFORD, J. B. & HARLAND, R. M. 2001. Xenopus Dishevelled signaling regulates both neural and mesodermal convergent extension: parallel forces elongating the body axis. *Development,* 128**,** 2581-92.

WALLINGFORD, J. B., ROWNING, B. A., VOGELI, K. M., ROTHBACHER, U., FRASER, S. E. & HARLAND, R. M. 2000. Dishevelled controls cell polarity during Xenopus gastrulation. *Nature,* 405**,** 81-5.

WANG, A., MA, X., CONTI, M. A., LIU, C., KAWAMOTO, S. & ADELSTEIN, R. S. 2010. Nonmuscle myosin II isoform and domain specificity during early mouse development. *Proc Natl Acad Sci U S A,* 107**,** 14645-50.

WANG, J., HAMBLET, N. S., MARK, S., DICKINSON, M. E., BRINKMAN, B. C., SEGIL, N., FRASER, S. E., CHEN, P., WALLINGFORD, J. B. & WYNSHAW-BORIS, A. 2006a. Dishevelled genes mediate a conserved mammalian PCP pathway to regulate convergent extension during neurulation. *Development,* 133**,** 1767-78.

WANG, Y., GUO, N. & NATHANS, J. 2006b. The role of Frizzled3 and Frizzled6 in neural tube closure and in the planar polarity of inner-ear sensory hair cells. *J Neurosci,* 26**,** 2147-56.

WILLIAMS-MASSON, E. M., HEID, P. J., LAVIN, C. A. & HARDIN, J. 1998. The cellular mechanism of epithelial rearrangement during morphogenesis of the Caenorhabditis elegans dorsal hypodermis. *Dev Biol,* 204**,** 263-76.

WILLIAMS, M., YEN, W., LU, X. & SUTHERLAND, A. 2014. Distinct apical and basolateral mechanisms drive planar cell polarity-dependent convergent extension of the mouse neural plate. *Dev Cell,* 29**,** 34-46.

WU, G., HUANG, X., HUA, Y. & MU, D. 2011. Roles of planar cell polarity pathways in the development of neural [correction of neutral] tube defects. *J Biomed Sci,* 18**,** 66.

YAMANAKA, T., HORIKOSHI, Y., SUGIYAMA, Y., ISHIYAMA, C., SUZUKI, A., HIROSE, T., IWAMATSU, A., SHINOHARA, A. & OHNO, S. 2003. Mammalian Lgl forms a protein complex with PAR-6 and aPKC independently of PAR-3 to regulate epithelial cell polarity. *Curr Biol,* 13**,** 734-43.

YAMBEN, I. F., RACHEL, R. A., SHATADAL, S., COPELAND, N. G., JENKINS, N. A., WARMING, S. & GRIEP, A. E. 2013. Scrib is required for epithelial cell identity and prevents epithelial to mesenchymal transition in the mouse. *Dev Biol,* 384**,** 41-52.

YBOT-GONZALEZ, P., SAVERY, D., GERRELLI, D., SIGNORE, M., MITCHELL, C. E., FAUX, C. H., GREENE, N. D. & COPP, A. J. 2007. Convergent extension, planar-cell-polarity signalling and initiation of mouse neural tube closure. *Development,* 134**,** 789-99.

YEN, W. W., WILLIAMS, M., PERIASAMY, A., CONAWAY, M., BURDSAL, C., KELLER, R., LU, X. & SUTHERLAND, A. 2009. PTK7 is essential for polarized cell motility and convergent extension during mouse gastrulation. *Development,* 136**,** 2039-48.

YIN, H., COPLEY, C. O., GOODRICH, L. V. & DEANS, M. R. 2012. Comparison of phenotypes between different vangl2 mutants demonstrates dominant effects of the Looptail mutation during hair cell development. *PLoS One,* 7**,** e31988.

YU, J. C. & FERNANDEZ-GONZALEZ, R. 2016. Local mechanical forces promote polarized junctional assembly and axis elongation in Drosophila. 5.

ZARBALIS, K., MAY, S. R., SHEN, Y., EKKER, M., RUBENSTEIN, J. L. & PETERSON, A. S. 2004. A focused and efficient genetic screening strategy in the mouse: identification of mutations that disrupt cortical development. *PLoS Biol,* 2**,** E219.

ZOHN, I. E. 2020. Mouse Models of Neural Tube Defects. *Adv Exp Med Biol,* 1236**,** 39-64.

Figure 1. *Scrib* mutants display open neural tube and turning defects. A) Phase contrast images of E11.5 embryos, scale bar = 200μm, black arrows indicate ONT and white arrows indicate turning defect. (B) Table comparing percentage of closed neural tubes versus NTD in *Scrib* mutant embryos. Numbers in red are significantly different ($p<0.001$, Fisher's Exact test). C) Graph displaying distribution of phenotypes between *Scrib* mutants and controls where * marks significance $p<0.01$ determined by Chi-square test. n represents number of embryos analyzed for each genotype.

Figure 2. *Scrib* interacts genetically with *Vangl2^{Lp}*. A) Phase contrast images of E11.5 embryos, scale bar = 200μm. B) Table comparing percentage of closed neural tube versus NTD in E11.5 embryos. Numbers labeled with different letters are statistically different ($p<0.05$ determined by Fishers Exact test). C) Confocal images of Vangl2 localization in *Scrib^{rumz}* E8.5 embryos: top panels basal Z slice, middle panel apical Z slice, bottom panel Z projections oriented with basal surface on bottom and apical surface on top, scale bar = 20μm.

Figure 3. *Scrib^{rumz}* mutation affects narrowing, polarity of intercalation, and rosette resolution. A) Box and whisker plot of percent change in CE index (aspect ratio at the end of the movie over the aspect ratio at the start) per hour over 6-10 hours of live imaging movies of E8.0 mouse embryos fluorescently labeled with *mG/mT*. B) Graph summarizing percent change per hour in AP and ML dimensions of live imaging movies. Error bars represent min and max and n represents number of embryos analyzed and depicted as individual dots in plot. C) Graph summarizing total number of cell separations observed in the neural tissue. Error bars represent standard deviation. D) Cell rearrangements, categorized as arising from cell division, single cell intercalation, T1 process, and rosette resolution for each genotype. E) Graph showing rosettes categorized by the mechanism of resolution for each genotype. F) Graph representing the changes in cell cluster orientation during rosette resolution for each genotype. G) Representative images of types of rosette resolution. In the panels representing unproductive rosettes, rosette 1 and 2 represent pulsing rosettes, and rosette number 3 shows an unproductive junctional rearrangement resolution. Rosettes are marked with white * and each rosette cluster is outlined in black. H) Rose plots displaying the distribution of AP (60-90º), diagonal (30-60º), and ML (0-30º) neural cell separations. Red bar represents circular mean. Genotypes labeled with different letters are statistically different ($p<0.05$ determined by Chi-square analysis).

Figure 4. Apical constriction is disrupted in *Scrib^{rumz}* mutants. A) Rose diagrams represent basal cell orientation where 90º indicates AP axis and 0º indicates ML axis. Uniformity was determined by Rao's U. The average basal cell aspect ratio (Basal AR) at the end of movies is listed below the p value where an aspect ratio of 1 represents a round cell. B) Graph indicates apical cell area at the start (1-3 somites) and end (6-8 somites, 6-10 hours) of live imaging movies of E8.0 embryos. C) Graph of apical constriction index (ACI), the ratio of basal cell area over apical cell area, at the start and end of live imaging movies. Error bars represent standard deviation. * indicates significance between start and end within genotypes ($p<0.05$ determined by two-way ANOVA). Letters indicate significance of end area between genotypes and bars marked with different letters are statistically different ($p<0.05$ determined by two-way ANOVA). At least 250 wildtype, 320 *Scrib$^{rumz/+}$*, and 250 *Scrib$^{rumz/rumz}$* cells were analyzed.

Figure 5. *Scrib^{rumz}* mutants exhibit mislocalization of junctional proteins. A) Z slice of confocal images of whole mount staining for junctional proteins in E8.5 embryos. B) Image J line scans were used to measure mean fluorescent intensity at the junctions and the cytoplasm of neural cells. Error bars represent standard deviation. Bars marked with different letters are

statistically different and * indicates significance for junctional measurements ($p<0.01$ determined by two-way ANOVA).

Figure 6. *Scrib*^{rumz} mutants exhibit mislocalization of cytoskeletal proteins. A) Z slice of confocal images of whole mount staining for cytoskeletal proteins in E8.5 embryos. B) Image J line scans were used to measure mean fluorescent intensity at the junctions and the cytoplasm of neural cells. Error bars represent standard deviation. * indicates significance at junction and bars marked with different letters are statistically different ($p<0.01$ determined by one-way ANOVA).

Supplemental Figure 1. Protein expression in *Scrib* mutants. A) Representative western blots for Scrib (red) and tubulin (green) in *Scrib*^{rumz} (top) and *Scrib*^{Crc} (bottom) embryos. B) Western blots were analyzed with Image Studio and normalized to tubulin expression. Error bars represent standard deviation and bars marked with different letters are statistically different ($p<0.05$ determined by one-way ANOVA).

Supplemental Figure 2. *Scrib* interacts genetically with *Vangl2*^{Lp}. Graph displaying distribution of phenotypes between genotypes where * marks significance $p<0.0001$ determined by Chi-square test. Bars marked with different letters are statistically different ($p<0.01$ determined by Chi-square test.

Supplemental Figure 3. Overall tissue shape changes in the neural tube is due to cell shape changes and not cell number. A) Graph indicates number of cells within distortion diagrams at the start and end of live confocal movies and shows no counts are statistically different from one another. B) Plot of percent change in area of distortion diagrams per hour. n represents the number of movies analyzed. Error bars represent standard deviation.

Figure 1. *Scrib* mutants display open neural tube and turning defects.

A

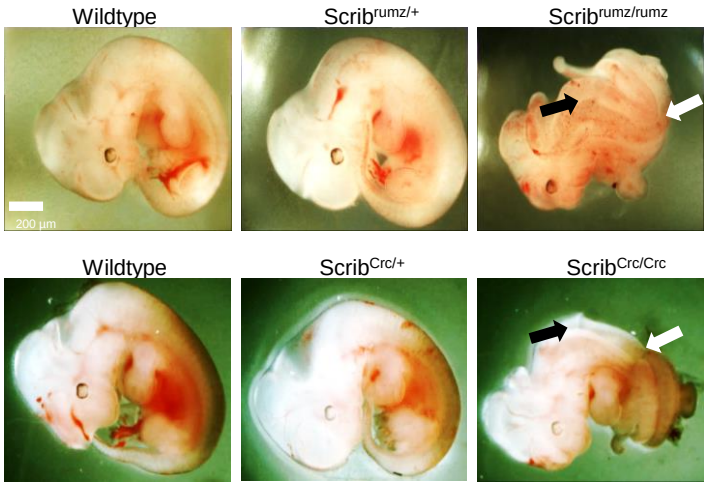

B

	% Closed Neural Tube	% Neural Tube Defect*
Wildtype	100	0
Scrib$^{rumz/+}$	96.4	3.6
Scrib$^{rumz/rumz}$	19.2	80.8
Wildtype	100	0
Scrib$^{Crc/+}$	98.0	2.0
Scrib$^{Crc/Crc}$	11.5	88.5

*open neural tube with or without turning defect

C

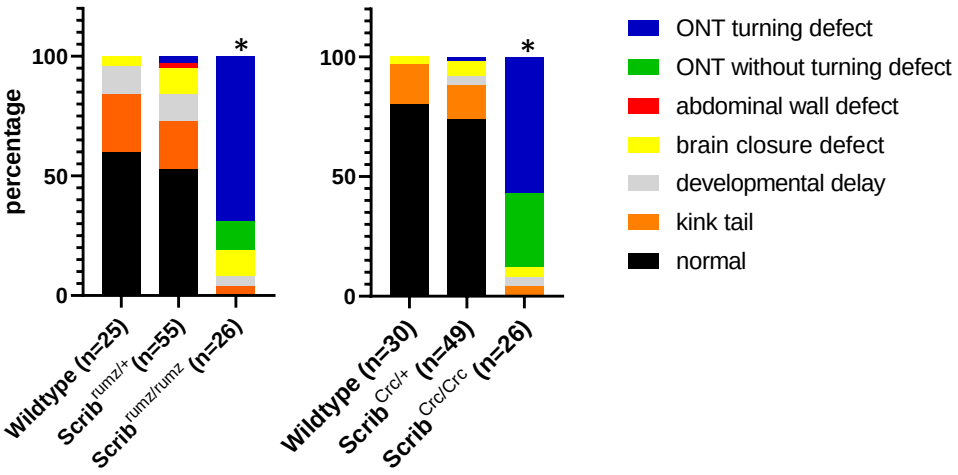

Figure 2. *Scrib* interacts genetically with *Vangl2*^{Lp}.

A

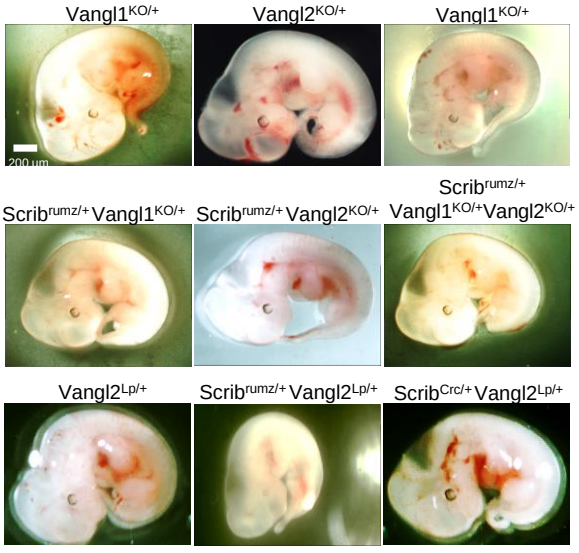

B

	% Closed Neural Tube	% Neural Tube Defect*
Vangl1$^{KO/+}$	100 ^{A}	0 ^{A}
Vangl2$^{KO/+}$	100 ^{A}	0 ^{A}
Vangl1$^{KO/+}$ Vangl2$^{KO/+}$	100 ^{A}	0 ^{A}
Scrib$^{rumz/+}$ Vangl1$^{KO/+}$	100 ^{A}	0 ^{A}
Scrib$^{rumz/+}$ Vangl2$^{KO/+}$	95.2 ^{AB}	4.8 ^{AB}
Scrib$^{rumz/+}$ Vangl1$^{KO/+}$ Vangl2$^{KO/+}$	94.4 ^{BD}	5.6 ^{BD}
Vangl2$^{Lp/+}$	96.4 ^{AB}	3.6 ^{AB}
Scrib$^{rumz/+}$ Vangl2$^{Lp/+}$	84 ^{C}	16 ^{C}
Scrib$^{Crc/+}$ Vangl2$^{Lp/+}$	87 ^{CD}	13 ^{CD}
*open neural tube with or without turning defect		

C

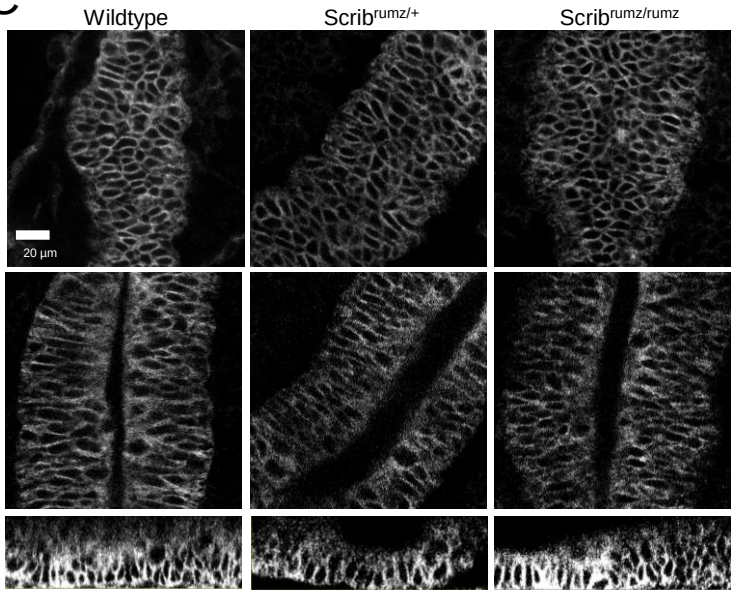

Figure 3. *Scrib*^{rumz} mutation affects narrowing, polarity of intercalation, and rosette resolution.

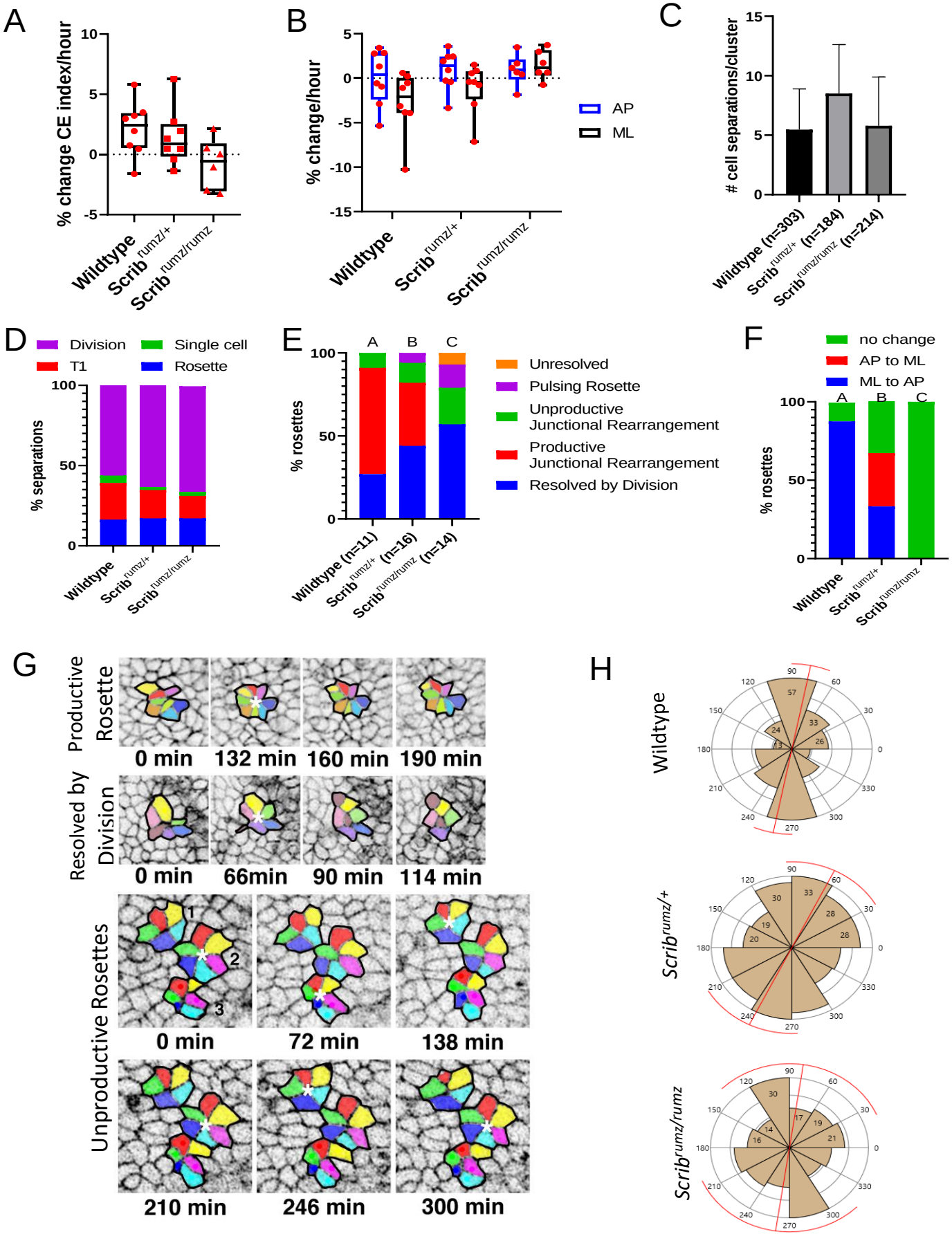

Figure 4. Apical constriction is disrupted in *Scrib*^{rumz} mutants.

A

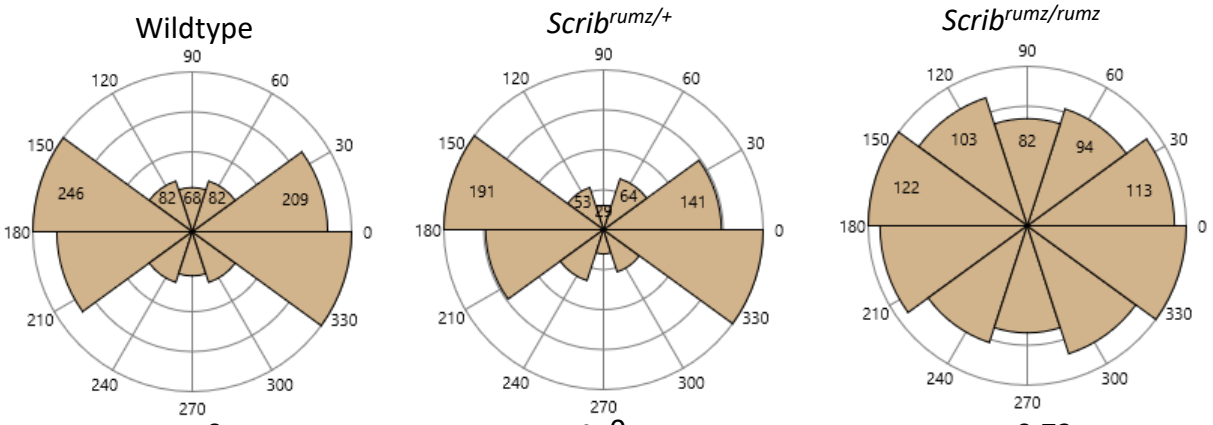

Wildtype: p=0, Basal AR= 1.78

Scrib$^{rumz/+}$: p=0, Basal AR= 1.85

Scrib$^{rumz/rumz}$: p=0.73, Basal AR= 1.58

B

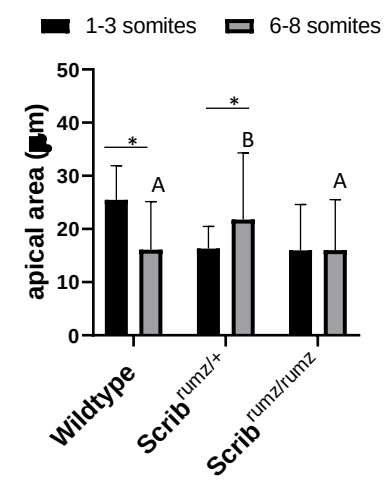

C

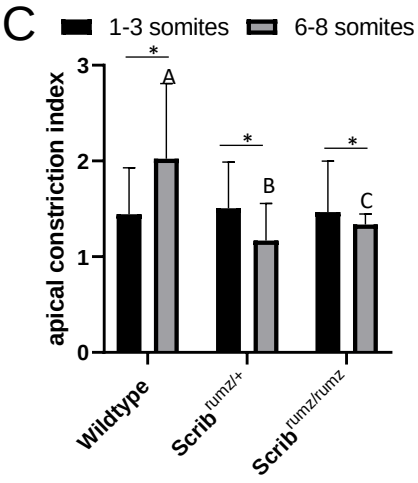

Figure 5. *Scrib*^{rumz} mutants exhibit mislocalization of junctional proteins.

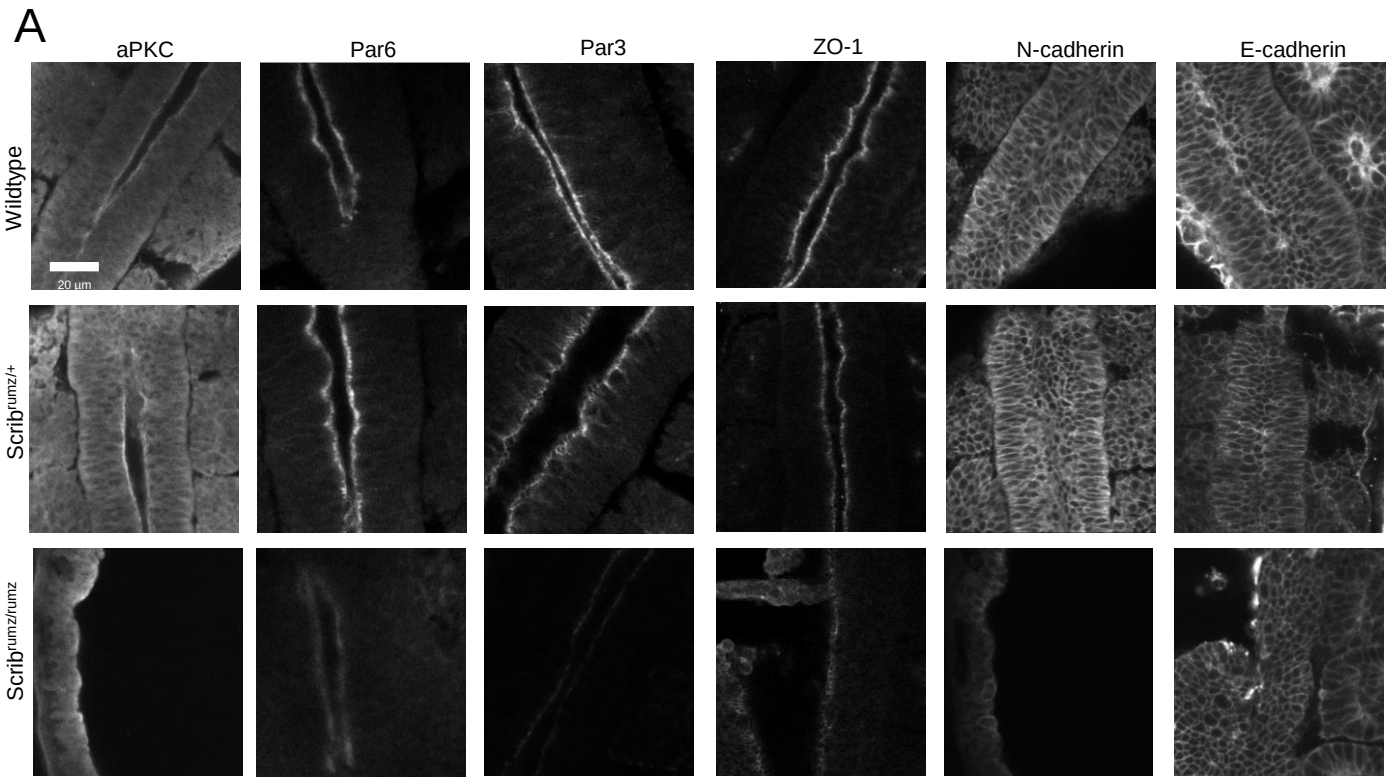

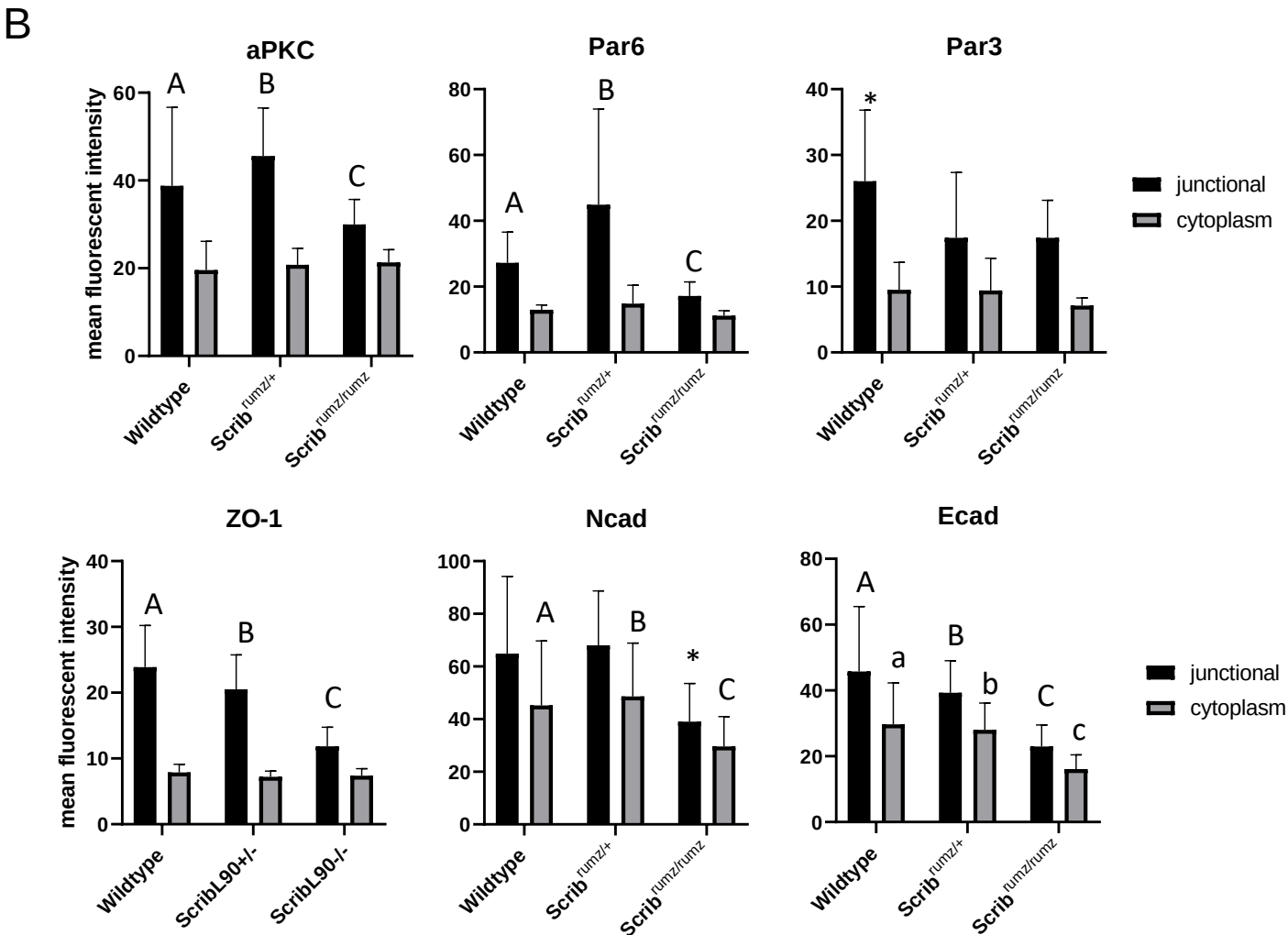

Figure 6. *Scrib*^{rumz} mutants exhibit mislocalization of cytoskeletal proteins.

A

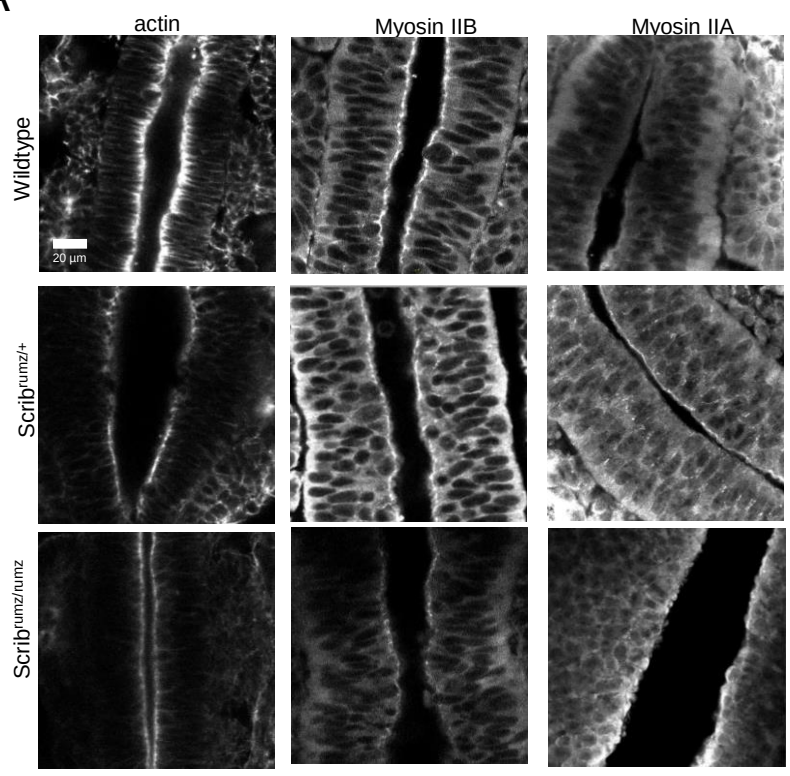

B

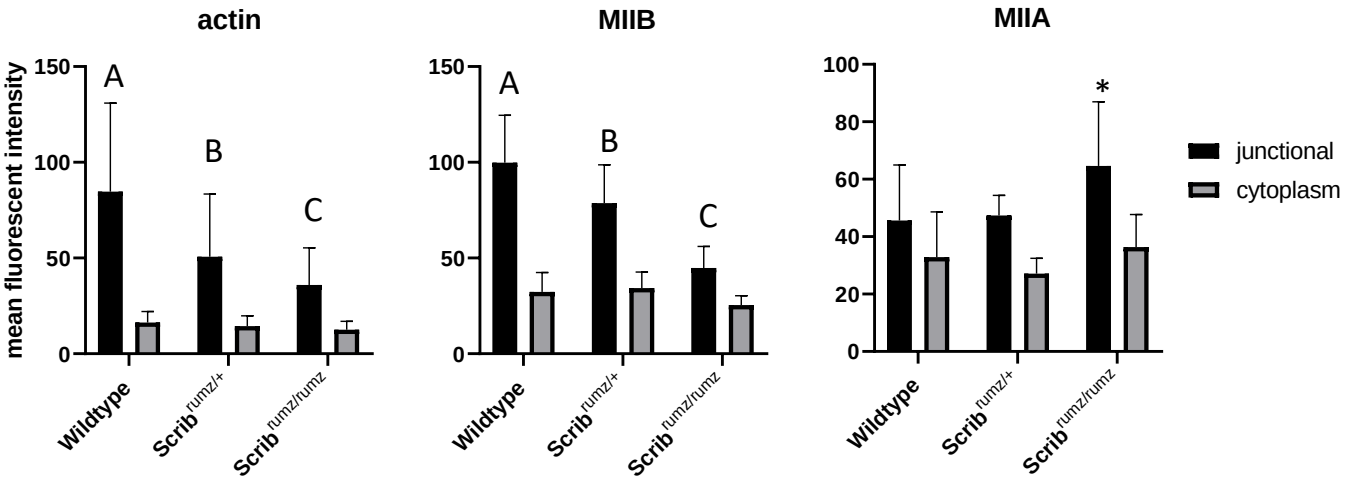

Supplemental Figure 1. Protein expression in *Scrib* mutants.

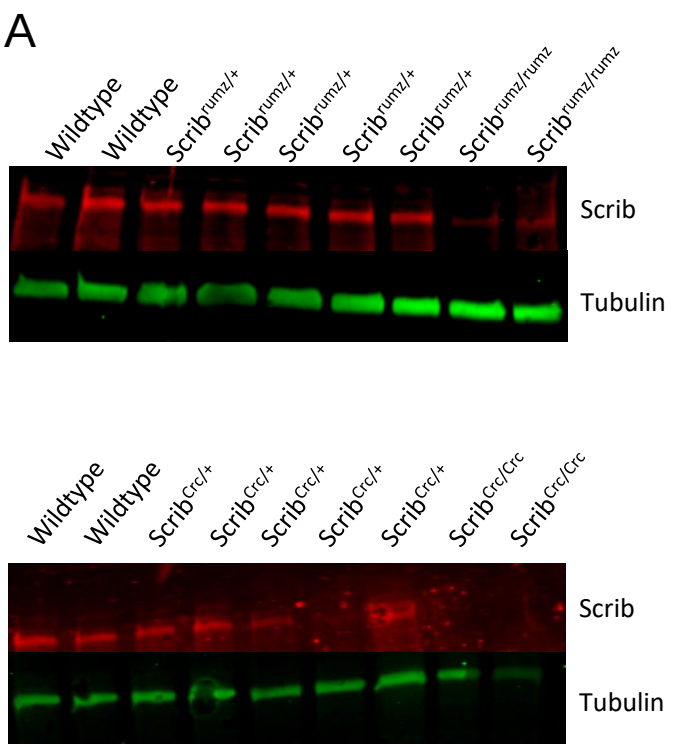

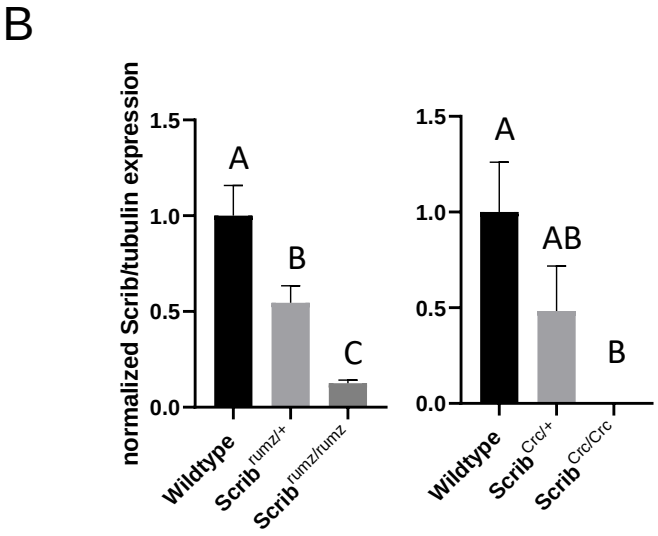

Supplemental Figure 2. *Scrib* interacts genetically with *Vangl2*^{Lp}.

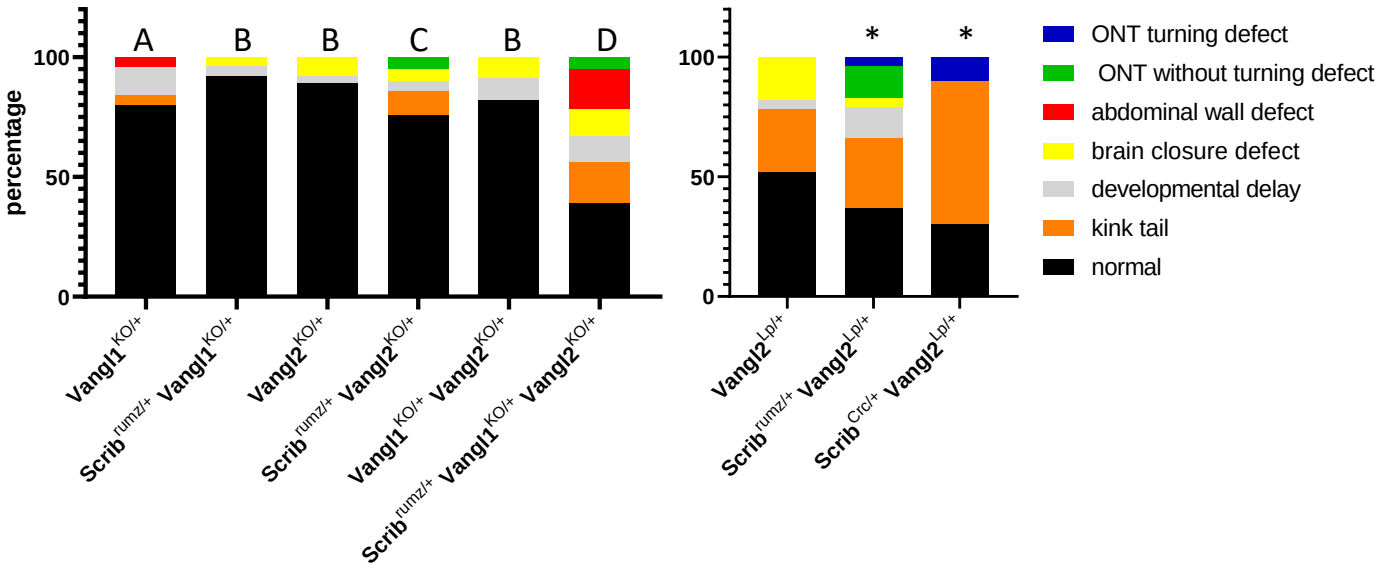

Supplemental Figure 3. Overall tissue shape changes in the neural tube are due to cell shape changes and not cell number.

A

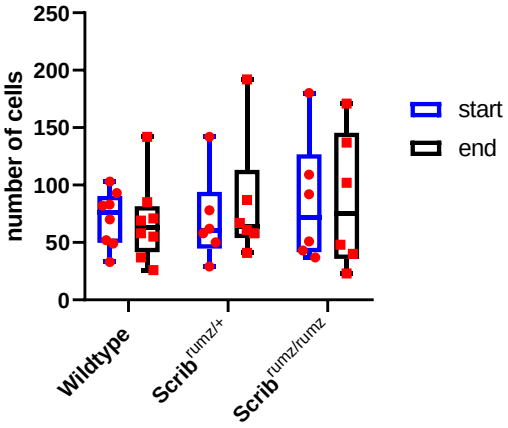

B

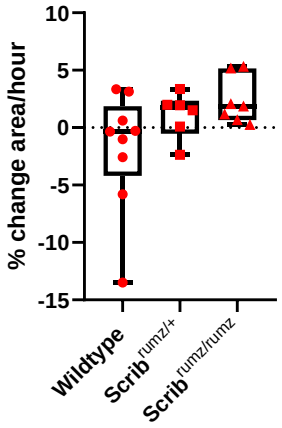

Supplementary Table 1. Genotyping Primers.

Mouse line	Sequence (5'-3')	Primer
Scrib^{rumz}	TGT GTG AGG TCA CTG AGG CCA T	Wildtype-F
	GCA CAC GCG CTT CTG TCC AA	Wildtype-R, mutant-R
	TCT GTG AGG TCA CTG AGG CAA A	Mutant-F
	ACACACGGGCTCTTTAACCC	Seq-F
	TCGGAGGACCTACATGCTCA	Seq-R
Scrib^{Crc}	CTT CAG CAT TGC TGG TGG	Mutant-F
	TGG GGA GGA ATG GGG IGG G	Mutant-R
	CTG ACT GCT GCT TCC CCT AC	oiMR7935-F
	TCC ACA GGG TAT GGT CCT TC	oiMR7934-R
Vangl2^{co}	GAA CAA TCC AAC GGG ACA CT	Vangl2-P1
	TCG ACA TGT GGT ATC TTT CCC	Vangl2-P2
	GCA GCT ATG ACC AGC TAC C	Vangl2-P3
Vangl1^{co}	ATC AAG CCC TAC AGG CAG ATG CTA AGA	PMS830-Wildtype
	ACA TGA TCA CAC CAA TTC TGT CCA	JN3371-Wildypte, mutant
	TCC TGT TTT ATG CTC TCT GCT CTG	JN3368-mutant
Vangl2^{Lp}	AAA CAG TCG ACC TTG GTG AA	Mutant-F
	AAG AGG AAG TAG GAC TGG CAG	Mutant-R
mT/mG	CGA GGC GGA TCA CAA GCA ATA	SG-wildtype
	CTC TGC TGC CTC CTG GCT TCT	SG-com
	TCA ATG GGC GGG GGT CGT T	SG-mutant
Sox2Cre	CTT GTG TAG AGT GAT GGC TTG A	Wildtype-F
	TAG TGC CCC ATT TTT GAA GG	Wildtype-R, TG-R
	CCA GTG CAG TGA AGC AAA TC	TG-F